minerals

MDPI

Article

Petrography, Geochemical Features and Absolute Dating of the Mesozoic Igneous Rocks of Medvedev and Taezhniy Massifs (Southeast Russia, Aldan Shield)

Alexey Ivanov, Evgeny Loskutov , Michil Ivanov and Anatolii Zhuravlev *

Diamond and Precious Metal Geology Institute, SB RAS, 39, prosp. Lenina, Yakutsk 677000, Russia
* Correspondence: ai.zhuravlevgeo@gmail.com; Tel.: +7-4112-33-56-59

Abstract: The paper presents the results of the petrographic and geochemical studies of igneous rocks of the Medvedev and Taezhniy massifs, including their first absolute dating. The massifs are located in central Nimnyr block of the n shield within the Leglier ore cluster of the Evotinskiy ore district (Southeast Russia, Aldan Shield). For the first time, the three-phase structure of the Medvedev massif has been defined, as observed in our expedition and petrographic studies. Rocks from the three phases of the Medvedev massif include quartz syenites, syenites, and monzonites, and rocks from the two phases of the Taezhniy massif include quartz monzonites and syenites. Geochemically, the rocks are close to volcanic island arcs, the formation of which was related by subducted oceanic crust of the Mongol–Okhotsk Ocean. The defined duality of the geochemical compositions of the igneous rocks of the massifs may be due to the presence of both mantle and crustal sources; however, it is most likely that these rocks resulted from the melting of a mixed mantle source or the latter was contaminated by the crust with further differentiation of melts in intermediate crust chambers. Additionally, geochemical characteristics suggest that the analyzed rocks are close to latite and shoshonite derivatives and can be considered as part of the monzonite–syenite formation type. The first identified periods of formation of igneous rocks in the Medvedev massif are 122.0–118.0 Ma and Taezhniy 117.5–114.5 Ma, which correspond to the Early Cretaceous (Aptian).

Keywords: Evotinskiy ore district; Leglier ore cluster; Aldan Shield; magmatism; massif; syenites; monzonites

check for updates

Citation: Ivanov, A.; Loskutov, E.; Ivanov, M.; Zhuravlev, A. Petrography, Geochemical Features and Absolute Dating of the Mesozoic Igneous Rocks of Medvedev and Taezhniy Massifs (Southeast Russia, Aldan Shield). *Minerals* **2022**, *12*, 1516. https://doi.org/10.3390/min12121516

Academic Editors: Antonios Koroneos, Ioannis Baziotis and Kristina Šarić

Received: 31 October 2022
Accepted: 24 November 2022
Published: 27 November 2022

1. Introduction

The study of the Mesozoic magmatism of the Aldan Shield began in the 20–30 s of the 20th century with the works of Yu. A. Bilibin, who described that the rocks in the Aldan complex formed in one volcanic cycle. In his works Yu. A. Bilibin refuted the hypothesis about the origin of the gold ore objects of the Aldan Shield in connection with Precambrian alaskite granites and proved their clear connection with Mesozoic alkaline rocks [1,2]. Recently, many authors have noted that the formation of alkaline rocks is accompanied by the appearance of the largest gold deposits [3–9]. Sillitoe [4] notes that about 20% of large gold deposits are associated with complexes of the shoshonitic and alkaline series. However, the rocks of these series are significantly inferior in volume to most of the main types of igneous rocks in terms of the scale of occurrence. Problems regarding the genesis and metallogenic specialization of multi-phase igneous formations in ore districts have been a topic of continuing debate [10–15]. One of the key points in solving these problems is a comprehensive study of each object, including their petrographic and geochemical features and age data in relation to the conditions of formation [12,13,16].

Alkaline rocks are formed in conditions of continental crust and island arcs associated with subduction processes and are known in many parts of the world. This paper presents the result of the study of the alkaline rocks of the Medvedev and Taezhniy massifs located in the central part of the Aldan Shield. In the opinion of the authors the formation of these massifs also occurred in the conditions of a volcanic arc associated with the subduction and closing of the Mongolian–Okhotsk paleoocean [17].

The Medvedev and Taezhniy massifs represent the multi-phase igneous formations of the Mesozoic tectonic–magmatic activation in the Evotinskiy gold-bearing ore district in the territory of the Leglier ore cluster (Southeast Russia, Aldan Shield) [18]. These have not been adequately studied until recently. Such multi-phase Mesozoic igneous structures are genetically related to gold occurrences and deposits at the adjacent central Aldan ore district [1,15,17,19–24].

2. Geological Setting

The Aldan Shield is located on the southern margin of the Siberian Platform and is composed mainly of deeply altered rocks of granulite, amphibolite and greenschist metamorphic facies. Five terranes are defined within the shield, including the West Aldan granite–greenstone composite terrane and the Central Aldan and East Aldan super-terranes separated by zones of tectonic mélange [17]. The southern part of the shield hosts the Tyndinsky tonalite–trondhjemite and Chogarsky granulite–orthogneiss composite terranes [17] (Figure 1). In the Mesozoic period of tectonic-magmatic activation on the territory of the Aldan Shield, a wide range of igneous rocks were intruded—ultra-alkaline, alkaline, subalkaline and alkaline earth from ultrabasic to acidic. The occurrences of magmatism of this phase are associated with orogeny in the nearby Mongolian–Okhotsk folded area on the southern active margin of the Mesozoic paleocontinent. In terms of its geodynamic position in the Mesozoic, the Aldan shield corresponds to the rear zones of the paleo-continent–ocean boundary with typical intraplate rift magmatism [21].

The Evotinskiy ore district is located in central Aldan Shield, spatially coincident with the Central Aldan superterrain. It is bordered on the west by the West Aldan multicomponent terrain along the Amga tectonic mélange and on the east by the Uchur terrain along the Tyrkandin tectonic mélange. It includes Nimnyr and Sutam multi-component terrains separated by the Seym overthrust [17] (Figure 1A).

The area of the ore district comprises ultrametamorphic rocks of the Precambrian basement, represented by biotite-pyroxene-amphibole, sillimanite-garnet-cordierite gneisses and crystalline schists with horizons, interlayers and lenses of quartzites, marbles, and calciphyres. Precambrian formations are granitized in varying degrees and host intrusions of Late Archean–Early Proterozoic granites and metabasites. The rocks are intensely dislocated with the formation of a complex system of folds and faults hosting numerous and extended late Proterozoic dolerite dykes. Carbonate Vendian–Lower Cambrian and terrigenous Lower Jurassic formations of the platform cover have been preserved in an insignificant volume. Mesozoic alkaline and calc–alkaline igneous rocks are represented by numerous sills, stocks (Evotinskiy, Medvedev, Taezhniy, Spartak) and syenite–porphyry dikes. The latter are spatially and genetically accompanied with low-temperature metasomatites (gumbeites, beresites) where during geological surveys, gold mineralization points have been found [25]. Next, follows a review of the geological structure of the two studied massifs of the Mesozoic stage of tectonic-magmatic activation.

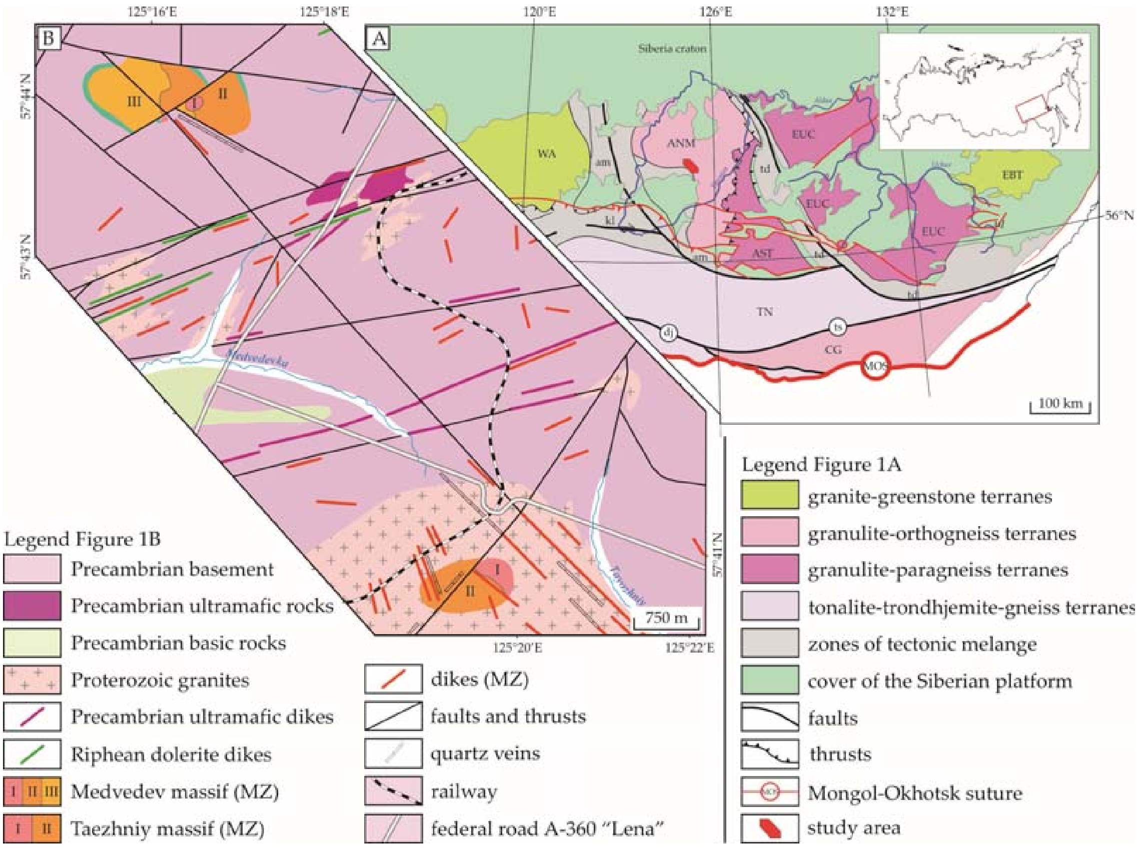

Figure 1. (**A**) Tectonic scheme of Aldan Shield [17]. Terranes: WA—West Aldan; EBT—Batomga; ANM—Nimnyr; CG—Chogar; AST—Sutam; EUC—Uchur; TN—Tyndin; zones of tectonic mélange: am—Amga, kl—Kalar, td—Tyrkanda; faults: dj—Dzheltulaksky, ts—Taksakandin. (**B**) Geological scheme of location of studied area (according to [18,26] with changes and additions of the authors).

The Medvedev and Taezhniy massifs intrude a Precambrian crystalline sequence (Figure 1B), which is a package of alternating, consonant, subparallel, compositionally contrasting linear sheet-like bodies composed of hypersthene and aluminous gneisses of the Nimnyr suite, rocks of the Medvedev Precambrian complex and subalkaline and normal biotite granites [17,27]. According to previous data [26], the massif is represented by augite-hornblende and hornblende syenite porphyry. During our expedition, we first uncovered that the massif has a three-phase structure that involves syenites, pyroxene-amphibole syenites and quartz monzonites.

The Taezhniy massif at the current level of the erosional cut has the shape of an irregular ellipsoid, with its long axis facing the northeast (Figure 2). Our expedition was the first to define its two-phase structure represented by quartz monzonite and syenites (Figure 2). The contacts found between rock differences are even and clear. Rocks of the massif intrude Precambrian granites (Figure 1B) and are intruded by bostonite and vogesite dikes (for the detailed description of the geology of small bodies associated with the Taezhniy massif see [26]).

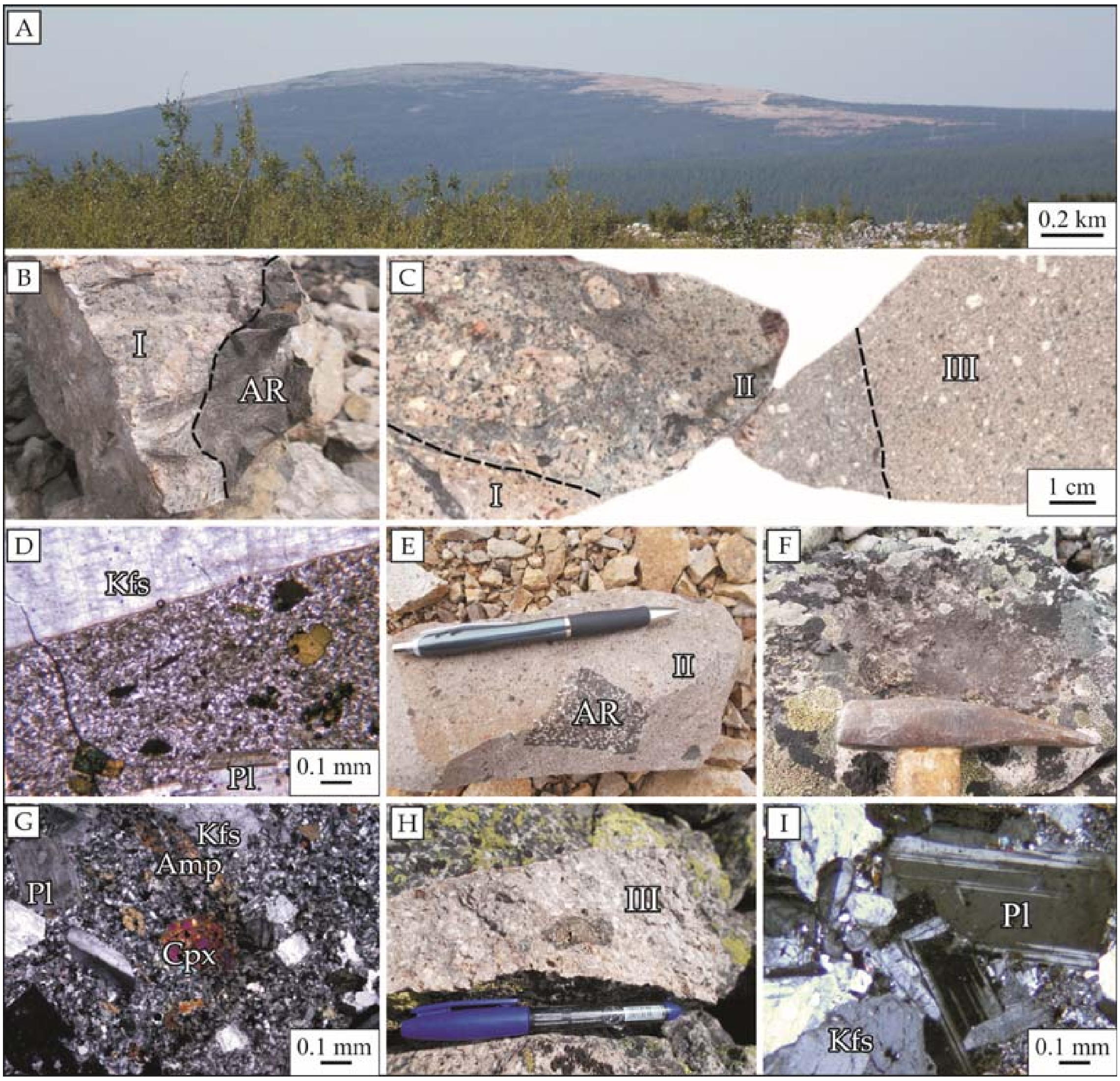

Figure 2. General view and petrography of rocks of the Medvedev massif. Rocks involved in the structure of the Medvedev massif: I—porphyry syenite, II—pyroxene-amphibole syenite, III—quartz monzonite, AR—Precambrian host rocks of basement, Qz—quartz, Amp—amphibole, Pl—plagioclase, Kfs—potassium feldspar, Cpx—clinopyroxene; (**A**) general view of Medvedev massif; (**B**) rocks of first phase of intrusion with xenolith of Precambrian schist; (**C**) contact between phases of massif; (**D**) thin section I19–19/4, porphyry syenite, phenocryst of Kfs larger 2 cm, magnification 40×, crossed nicols; (**E**) rocks of second phase with xenoliths of Precambrian schists; (**F**) miarols in rocks of second and third phases of intrusion; (**G**) thin section I19–10, pyroxene–amphibole syenite, phenocrysts Cpx and Amp, mag. 40×, nicols +; (**H**) rocks of third phase; (**I**) thin section I19–16, quartz monzonite, euhedral crystals Pl with anhedral crystals of Kfs, mag. 40x, nicols +.

3. Materials and Methods

We collected samples for the study during the expedition in 2018 to 2020. Petrographic composition was studied using a polarized light microscope MIN-8 (JSC LOMO, St.Petersburg, Russia), (70 thin sections). The photographs of the thin sections were made using a polarized light microscope Olympus BX 50 (Leica Camera AG, Wetzlar, Germany), with 25×, 40× and 100× magnifications, and a Zeiss Axio CamICc 3 camera (Carl Zeiss AG, Oberkochen, Germany). Major components and microelements were identified using silicate analysis (L.T. Galenchikova) (SF-56, JSC LOMO, St. Petersburg, Russia) and multi-element atomic emission spectroscopy (S.Yu. Korkina) (LTD VMK-Optoelectronika, Moscow, Russia) at the Department of Physicochemical Analyses (laboratory of DPMGI SB

RAS, Yakutsk, Republic of Sakha, Russia). Seventy samples were analyzed. Microelements (25 samples) were identified using a mass spectrometer ELAN, DRC-e (LTD CAC Plasma, Tomsk, Russia).

The analysis of the Rb-Sr isotopic systems of rocks was performed using the isotopic dilution method to determine the concentrations of rubidium and strontium. To achieve this, weighed amounts of mixed indicators $^{85}Rb-^{84}Sr$ were added to pre-ground sample portions. Prepared samples were then decomposed in a mixture of nitric and hydrofluoric acids. The isolation of rubidium and strontium for isotopic analysis was carried out by cation exchange chromatography on AG50W-X8 resin (Bio-Rad Laboratories Inc., Hercules, CA, USA). Isotope dilution analysis was applied to determine the quantity of rubidium and strontium in Rb-Sr isotopic systems of rocks using a multiple collector mass spectrometer TRITON (LTD Thermotest Finnigan MAT, Bremen, Germany) in static mode. The $^{88}Sr/^{86}Sr$ = 8.37521 ratios were normalized to correct for Sr-isotope fractionation. The ratios were normalized to $^{87}Sr/^{86}Sr$ = 0.71025 for NBS 987. Rb and Sr determinations were accurate to 0.5%. Blanks were 30pg for Rb and 30pg for Sr.

U-Pb zircon dating was performed using SIMS SHRIMP-IIe (LTD ASI, FYSHWICK, ACT, Australia) (Secondary Ion Mass-Spectrometry by a Sensitive High-Resolution Ion Micro Probe) at the Center for Isotope Studies of the A.P. Karpinsky Russian Geological Research Institute (FGBU "VSEGEI"). Next, the sequence of dating methods used is described.

Representative zircon grains were analyzed along with reference material TEMORA and 91500. Analyses were recorded in the scanning electron microscope CamScan MX2500 (CamScan Electron Optics Ltd, Cambridge, United Kingdom) with the CLI/QUA2 system to obtain CL and BSE images. The operating distance was 25–28 mm, accelerating voltage 20 kV, and the nearly full beam current into the Faraday cup was 4–6 nA. Current value was varied to obtain the maximum contrast of CL images and to minimize the surface corrosion of the disc resulting from local heating.

U-Pb ratios were measured following the method adapted in A.P. Karpinsky Russian Geological Research Institute (FGBU "VSEGEI") [28], as described in [29]. The intensity of the primary molecular oxygen beam was 4nA, and the size of the sampling crater was 20×25 μm with depth up to 2 μm. The data were processed using SQUID software (Berkeley Geochronology Center, Berkeley, CA, USA) [30]. The U-Pb ratios were normalized to the value 0.0668 of the standard zircon TEMORA, which corresponds to its age of 416.75 ± 0.24 Ma [31]. The zircon standard 91500 with U content 81.2 ppm and $^{206}Pb/^{238}U$ age of 1062 Ma [32] was used as a concentration standard. The Raster one-minute cleaning of a rectangular (50×65 μm) section of mineral prior to dating allowed the minimization of surface contamination.

Individual analyses (of ratios and ages) are reported with 1σ error, and the calculated ages, including concordant, indicate 2σ errors. Ahrens–Wetherill diagrams with Concordia [33] were plotted using ISOPLOT/EX (Berkeley Geochronology Center, Berkeley, CA, USA) [34]. Non-radiogenic plumbum correction was applied based on the measured ^{204}Pb and the modern plumbum isotopic composition of the Stacy–Kramers model [35].

4. Results

4.1. Petrography

First phase syenites of the Medvedev massif intrusion (Figure 2A,B) are least common and come as light gray pinkish leucocratic varieties with a large-porphyry structure, with K-feldspar and plagioclase phenocrysts being up to 3–5 cm. The rocks show a massive texture. The rocks of the first phase of intrusion have xenoliths of host rocks (Figure 2B). Numerous blocks of xenogenic crystalline schists were found in the central part. Contacts with subsequent phases are clear, sharp and without facies transitions (Figure 2C). The crystal optical porphyry structure resulted from the presence of phenocrysts of K-feldspar and plagioclase (Figure 2D), and the rocks also demonstrate elements of monzonite structure (idiomorphism of plagioclase relative to K-feldspar). The fine-grained groundmass lacks diagnostic evidence. The rocks of the phase show traces of secondary changes. The petrographic composition (hereafter, the composition is described in detail in [18]) demonstrates a predominance of K-feldspar 60% over plagioclase 30%, and in the dark-colored group of minerals, a predominance of amphibole 8% over pyroxene 1% is seen and the ore mineral content makes up to 1%.

The rocks of the second phase occupy most of the area of the massif (Figure 1B) and are represented by gray, gray-pinkish pyroxene–amphibole syenites with hypidiomorphic granular and porphyry structure. The rocks have a massive texture. The formations of the phase have the numerous xenoliths of crystal schists, Archean microcline granites, as well as rocks of the previous phase (Figure 2E). The rocks contain a significant number of miaroles of various sizes (from 20 cm to 1 m in diameter) (Figure 2F). The composition is dominated by K-feldspar 60%, with 20% of plagioclase, an approximately equal amount of basic dark-colored minerals, pyroxene 6% and amphibole 8%, and the content of both biotite and quartz is significantly less than 1%, while the content of ore minerals is up to 4% (Figure 2G). The geological age of the rocks was determined from clear contacts with other phases of the massif, as well as from the xenoliths of the first phase rocks.

The third phase rocks of the massif are represented by gray monzonites (Figure 2H). The clear idiomorphism of plagioclase relative to K-feldspar as well as the presence of idiomorphic plagioclase crystals included in K-feldspar grains determines the monzonite structure (Figure 2I). The rocks have a massive texture. The rocks of the phase as well as the pyroxene–amphibole syenites show miaroles, albeit in a smaller amount. The third phase rocks of the intrusion of the massif are characterized by the predominance of plagioclase up to 50% over K-feldspar with up to 25%. Mafic minerals are not distributed uniformly, with a significant predominance of 16% hornblende over 2% pyroxene. The main fine-grained mass consists of hard-to-diagnose feldspar and 2% fine biotite. The rocks also contain up to 2% of quartz. The amount of ore mineral is up to 3%.

The least abundant rocks of the Taezhniy massif (Figures 1B and 3A) are dark gray monzonites (Figure 3B), which form a small outcrop in its northeastern part and represent the first phase of intrusion. The porphyry structure results from the presence of K-feldspar and plagioclase phenocrysts up to 5 mm in size (Figure 3B). The rocks have a massive texture. The groundmass is fine-grained (Figure 3C). The mineral composition features a predominance of plagioclase 60% over KFS 20%, amphibole 8% over pyroxene 2%, quartz content at 6%, apatite and zircon content of 2% and 2% ore minerals. The rocks of the phase show traces of secondary changes (pelitization, seritization and chloritization).

The light gray essential syenites of the second phase (Figure 3D) are the most widespread over the area of the massif (Figure 1B). They are characterized by a hypidiomorphic granular structure and a massive texture (Figure 3E). The petrographic composition of the least altered varieties defined the predominance of K-feldspar 60% over plagioclase 30%, amphibole 3% over pyroxene 1%, biotite content 1% and quartz up to 5%. The rocks of the phase are characterized by the presence of trace of secondary change—pelitization, sericitization and chloritization. In the southwestern part of the massif, the fragments of metasomatites along Archean granites contain single druses and brushes of quartz, the rocks of the phase are significantly quartz-flooded.

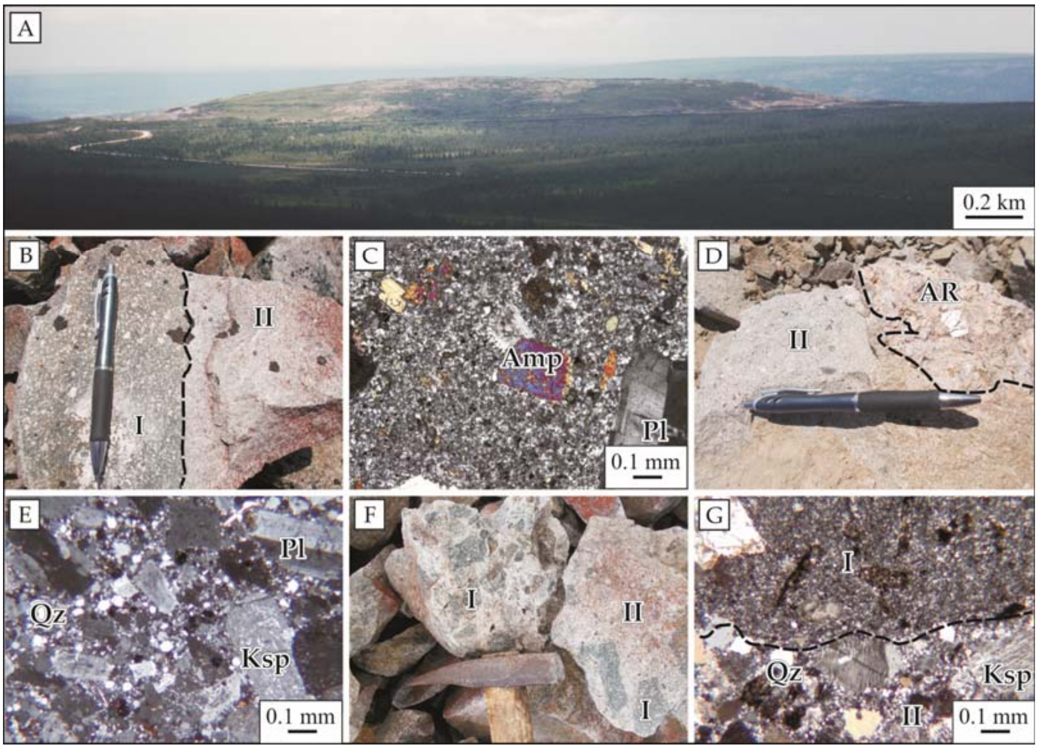

Figure 3. General view and petrography of rocks of the Taezhniy massif. Rocks involved in the structure of the Taezhniy massif: I—quartz monzonites, II—syenite, AR—Precambrian host rocks of basement, Qz—quartz, Amp—amphibole, Pl—plagioclase, Kfs—potassium feldspar, Cpx—clinopyroxene; (**A**) general view of Taezhniy massif; (**B**) contact between two phases of massif; (**C**) thin section I19–24/2, phenocrysts Amp and zoned Pl in quartz monzonites of Taezhniy massif, mag. 40×, crossed nicols; (**D**) contact between rocks of second phase and Precambrian host rocks of basement; (**E**) thin section I19–27/6, pelitized Kfs in syenite, mag. 40×, nicols +; (**F**) xenoliths of monzonites (I phase) in syenite, mag. 10×, nicols +; (**G**) thin section I19–24, xenolith of monzonites (I phase) in syenite, mag. 10×, nicols +.

4.2. Geochemical Composition

In terms of total alkaline content ($Na_2O + K_2O$) syenites of the first phase of Medvedev massif are classified as subalkaline rock 8.15%–11.88% [36] with higher K_2O (4.35%–6.59%) than Na_2O content (3.8%–5.29%) (Table A1). They are potassic alkaline ($Na_2O/K_2O < 1$) rocks of the high-aluminous (al′ = 2.19) with AG coefficient being 0.80 (Table A1). According to the diagram ($Na_2O + K_2O$)-SiO_2 [37] the rocks of the mass are classified as syenites (Figure 4A). In the R_1-R_2 diagram [38] they fall between subalkaline and quartz syenites (Figure 4B). Their K_2O–SiO_2 ratio [39] corresponds to the shoshonitic petrochemical series of igneous rocks (Figure 4C). Geochemically, the first phase rocks of the Medvedev massif are specified into Rb, Ba, Sr, B, Cr, V, Nb, Sc (Table A2), i.e., lithophile elements, with the content of both chalcophile Cu, Sn, Zn Pb, Ge and siderophile Ni and Co elements being significantly lower. The high content of Rb (85.50–107.10 ppm), Ba (1260–3100 ppm) and Sr (760–1010 ppm) as well as concentrations of Zn (53.20–100 ppm) and Co (4.51–6.54 ppm) suggest that syenites of the first phase are closest to latite derivatives [40]. The rocks demonstrate a negative [41] gently inclined REE pattern, i.e., they are cerium-rich (La, Ce, Pr, Nd, Sm, Eu) and yttrium-poor (Y, Gd, Tb, Dy, Ho, Er, Tm, Yb, Lu) (Table A3, Figure 4D). The ratios La/Yb = 16.01–18 and Ce/Yb = 31.57–33.44 in syenites of the massif are close to those of the latite series [40].

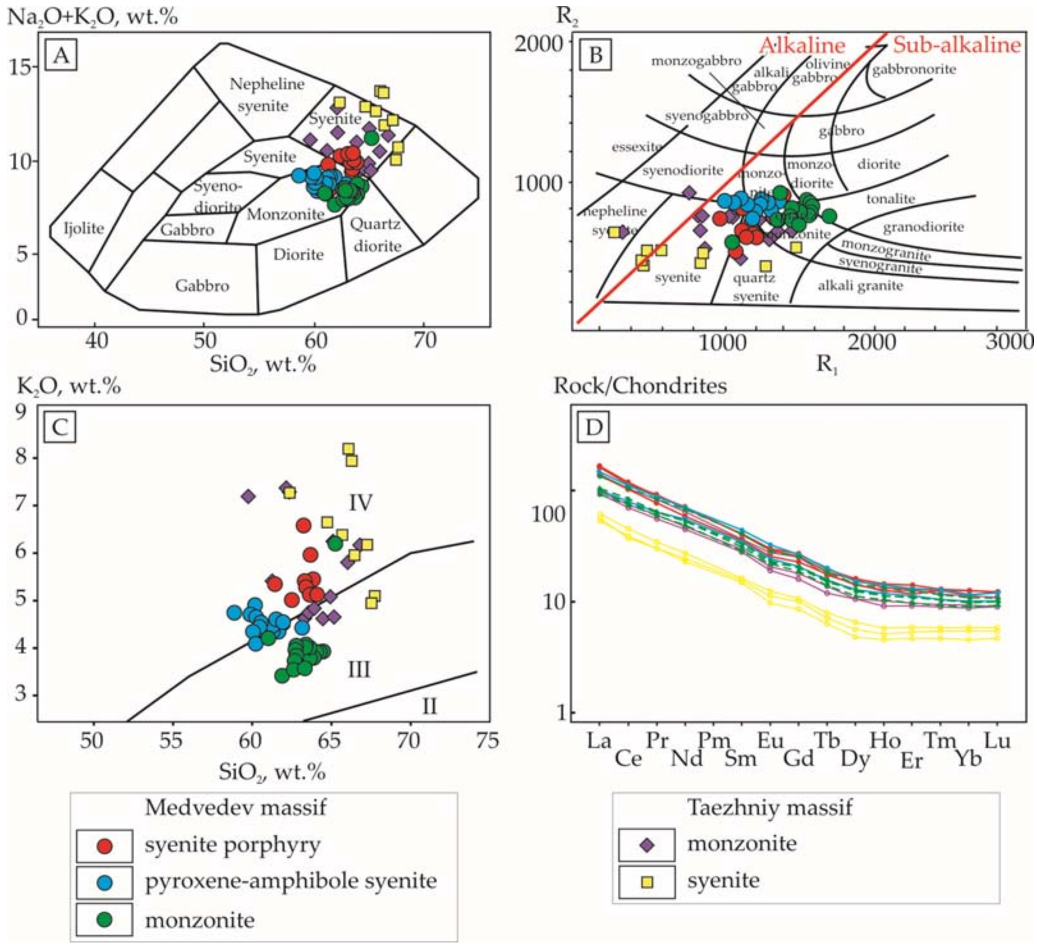

Figure 4. Classification diagrams for igneous rocks of the Medvedev and Taezhniy massifs. (**A**) diagram (Na_2O + K_2O) − SiO_2 [42], adopted for plutons by [37]; (**B**) diagram (R_1 − R_2) [38]. R_1 = 4Si − 11(Na + K), R_2 = 6Ca + 2Mg + Al; (**C**) K_2O–SiO_2 diagram [39], fields: II—medium-potassium calc-alkaline, III—high-potassium calc-alkaline, IV—shoshonite; (**D**) distribution of REE elements, normalization to chondrite [41].

Syenites of the second phase, unlike the previous phase, are characterized by slightly lower values of SiO_2 58.81%–63.06%, Al_2O_3 14.81%–16.41%, MgO 1.1%–2.68% and relatively high values of TiO_2 0.51%–0.78%, Fe_2O_3 2.27%–4.18%, MnO 0.11%–0.16% and CaO 3.34%–4.71%, as well as lower total alkalinity (Na_2O + K_2O) = 7.72%–9.69% corresponding to subalkaline rocks [36] with a slight predominance of K_2O 3.95%–4.91% over Na_2O 3.77%–4.78% (Table A1). According to the Na_2O/K_2O > 1, they are close to potassium-sodium alkaline and high-aluminous al′ = 1.42 rocks with AG coefficient 0.78 (Table A1). According to the diagram (Na_2O + K_2O) − SiO_2 [37], the rocks of this phase fall between syenites and monzonites (Figure 4A). Their R_1–R_2 ratio [38] also ranges from subalkaline syenites to quartz monzonite (Figure 4B). According to the K_2O–SiO_2 ratio [39] they belong to the shoshonitic igneous series as well as those of the previous phase (Figure 4C). The syenites of the second phase, in contrast with earlier phase, have a relatively high content of both siderophile and lithophile elements (Table A2). In terms of Rb (71.48–113.36 ppm), Ba (1000–2800 ppm), Zr (120–270 ppm), Sr (590–1100 ppm), Nb (3.66–10.60 ppm) and Co (9.15–20 ppm) content they are closest to latite derivatives [40]. The REE pattern is close to that of the previous phase but differs in a somewhat higher concentration of light elements (Table A3, Figure 4D). The ratios La/Yb = 16.01–18 and Ce/Yb = 31.57–33.44 (Table A3) correspond to the latite series [40].

The third phase monzonites of the massif in terms of SiO_2 content (61.13%–64.43%) are close to syenites of the first phase but differ in relatively high content of Al_2O_3 15.09%–16.81%, TiO_2 0.28%–0.65%, Fe_2O_3 1.32%–4.54% и CaO 3.27%–4.76% (Table A1) as well as low values of MnO 0.08%–0.13%, MgO 0.05%–3.33% and alkalinity ($Na_2O + K_2O$) = 7.87%–8.89%, where Na_2O 4.25%–4.99% dominates over K_2O 3.46%–4.25% (Table A1). The $Na_2O/K_2O > 1$ ratio corresponds with potassium-sodium alkaline, high-aluminous al′ = 1.94 rocks with AG coefficient 0.72 (Table A1). According to the diagram ($Na_2O + K_2O$)-SiO_2 [37], the rocks of this phase are classified as monzonites (Figure 4A). In the R_1–R_2 ratio [38] the composition points almost fully come within the field of subalkaline quartz monzonites, with most altered residual partially falling into the field of monzodiorites and tonalities (Figure 4B). Their K_2O-SiO_2 ratio [39] corresponds to the high-potassic, calcareous–alkaline petrochemical series (Figure 4C). The geochemical composition of monzonites, in contrast to rocks of earlier phases, is characterized by the lower content of chalcophile elements (Table A2). At the same time, in contrast to previous rocks, they demonstrate a somewhat higher content of lithophile elements and lower Cr, V, Ba and Rb (Table A2). In terms of Rb (61.20–91.80 ppm), Ba (1500–2000 ppm), Sr (780–1060 ppm), Zr (120–190 ppm), Nb (5.32–10.80 ppm) and Ni (7.99–14 ppm) content, they are closest to latite derivatives [40]. The REE pattern of quartz monzonites is close to that of the previous phases of the massif but differs in the lower concentration of both heavy and light elements (Table A3, Figure 4D). The ratios La/Yb = 13.97–17.10 and Ce/Yb = 27.16–34.61 (Table A3) in quartz monzonites are close to syenites of the second phase of the massif and belong to the latite series [40].

By total alkalinity ($Na_2O + K_2O$) the *early phase quartz monzonites* of the Taezhniy massif belong to subalkaline rocks 9.23%–12.83% [36], with K_2O 3.79%–7.29% as slightly higher than Na_2O 3.92%–6.15% (Table A1). They are potassium alkaline $Na_2O/K_2O < 1$, high-aluminous al′ = 1.14–4.13 rocks with AG coefficient 0.82–1.13 (Table A1). According to the diagram ($Na_2O + K_2O$)-SiO_2 [37], the rocks of this phase plot in syenites and monzonites field (Figure 4A). In the R_1–R_2 ratio [38] the composition points come between subalkaline syenites and quartz monzonites (Figure 4B). According to the K_2O–SiO_2 ratio [39], they belong to the high-potassic, calcareous–alkaline, as well as shoshonitic petrochemical, series (Figure 4C). Geochemically, the first phase quartz monzonites of the Taezhniy massif are specified into lithophile elements Rb, Ba, Sr, B, Cr, V, Nb and Sc (Table A2). The content of both chalcophile Cu, Sn, Zn Pb, Ge and siderophile Ni and Co elements is significantly lower than that of lithophile. High Rb (66–223 ppm) and Sr (330–1100 ppm) content, extremely high Ba (1200–2700 ppm) and a concentration of Zr (81–160 ppm) and Co (4–15 ppm) make them closer to latite derivatives [40]. The rocks of the phase have a negative gently inclined REE pattern, i.e., they display a high abundance of light elements (La, Ce, Pr, Nd, Sm, Eu) and a low abundance of heavy elements (Y, Gd, Tb, Dy, Ho, Er, Tm, Yb, Lu) (Table A3, Figure 4D). The ratios La/Yb = 14.42–16.93 and Ce/Yb = 28.90–33.21 in quartz monzonites of the massif are close to those of the latite series [40].

The least altered residual of syenites of the late phase of the Taezhniy massif, unlike the previous rocks, are characterized by a somewhat higher content of SiO_2 and Al_2O_3 and a low content of TiO_2, Fe_2O_3, FeO, MnO, MgO and CaO (Table A1). The rocks of the phase differ from the formations of the previous phase by high total alkalinity ($Na_2O + K_2O$ = 10%–13.67%), which makes them subalkaline [36], where K_2O (4.91%–8.12%) dominates over Na_2O (5.09%–6.28%) (Table A1). The rocks are potassium alkaline $Na_2O/K_2O < 1$, belong to the high-aluminous series al′ = 2.51–5.70 with the AG coefficient 0.86–1.12 (Table A1). According to the diagram ($Na_2O + K_2O$)-SiO_2 [37], the rocks belong to syenites (Figure 4A). In the R_1–R_2 diagram [38], the composition points form a secant trend in the field of subalkaline rocks from syenites to quartz syenites (Figure 4B). According to the K_2O–SiO_2 ratio [39], syenites belong to the shoshonitic petrochemical series (Figure 4C). Rocks of the phase are distinguished from the earlier syenites by the content of both chalcophile and lithophile elements (Table A2). By the content of Rb (90–126 ppm), Ba (450–3000 ppm), Sr (230–1000 ppm), Zr (80.2–190 ppm), Nb (5.9–11.8 ppm) and Co (3.2–7.8 ppm) content, they are closest to latite derivatives [40]. The REE pattern of syenites is close to that of the first phase syenites but with lower concentrations of all elements (Table A3, Figure 4D). The ratios La/Yb = 13.50–17.14 and Ce/Yb = 25.83–29.67 (Table A3) are close to those of the latite derivatives [40].

4.3. Geochronology

The obtained concordant U-Pb age of syenites (calculated from six zircon points) is 122.0 ± 5.2 Ma (MSWD = 5.9, Figure 5A). The studied zircons are characterized by the low values of the ratio $^{232}Th/^{238}U$ from 0.15 to 0.40 (average 0.27), and the U content ranges from 170 to 1052 (average 590) and Th 65–148 (124) ppm, respectively (Table A4).

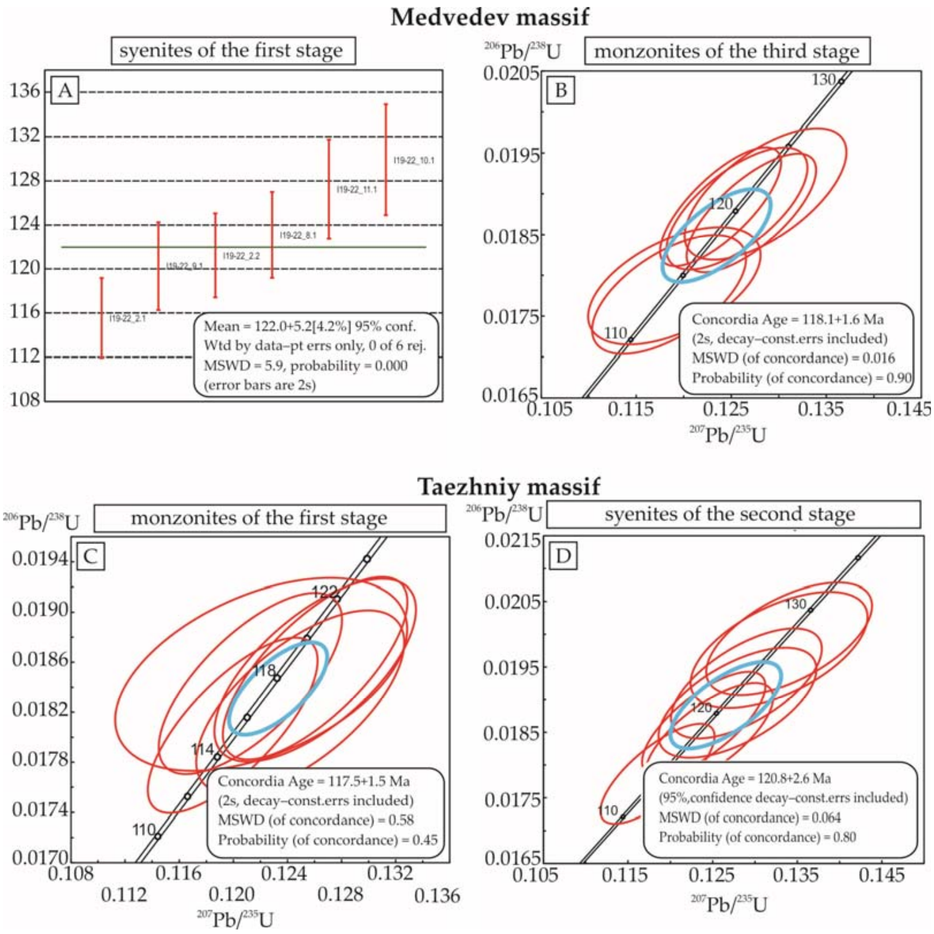

Figure 5. Age data of Medvedev and Taezhniy igneous rocks: (**A**) results of weighted mean $^{207}Pb/^{235}U$ age Ma of zircons from igneous rocks of first phase of Medvedev massif; (**B**) concordia diagram and weighted mean $^{207}Pb/^{235}U$ for sample I19-15(n = 6); (**C**) concordia diagram and weighted mean $^{207}Pb/^{235}U$ for sample I19-24(n = 6); (**D**) concordia diagram and weighted mean $^{207}Pb/^{235}U$ for sample I19-27(n = 7). Data point error ellipses are 2σ.

The obtained concordant U-Pb age of quartz monzonites (according to six zircon points) was 118.0 ± 1.6 Ma (MSWD = 0.016, Figure 5B). The studied zircons are characterized by significantly lower values of the $^{232}Th/^{238}U$ ratio from 0.01 to 0.02 (on average 0.01), as compared to those from the first phase rocks of the Medvedev massif. The U content is also much higher and ranges from 447 to 1237 (average 737) with low Th 4–20 (10) ppm (Table A4).

The obtained concordant U-Pb age of quartz monzonites of the Taezhniy massif based on six zircon points was 117.5 ± 1.5 Ma (MSWD = 0.58 Figure 5C). The studied zircons are characterized by higher values of the $^{232}Th/^{238}U$ ratio from 0.06 to 0.41 (0.25 on average) relative to zircons from the rocks of the Medvedev massif, and the content of U and Th is much higher compared to the latter at 304–1481 (average 825.20) and 38–345 (177.66) ppm (Table A4).

The obtained concordant U-Pb age of syenites (based on seven zircon points) was 120.8 ± 2.6 Ma (MSWD = 0.064, Figure 5D). The studied zircons are characterized by relatively low values of the $^{232}Th/^{238}U$ ratio from 0.005 to 0.33 (on average 0.17) in relation to the previous rocks (except for zircons of the 3rd phase of the Medvedev massif); the U content in them is also much higher, ranging from 486.29 to 1925.8 (average 1123.4), with Th 14.5–563.07 (255.17) ppm (Table A4). Despite the earlier values of the calculated concordant absolute age of the second phase rocks, the latter were identified as later formations according to geological relationships, and numerous xenoliths of quartz monzonites of the previous phase contained in the rocks (Figure 3F,G) were determined.

4.4. Formation Conditions

According to the Rb/Sr-SiO_2 [43] and $Al_2O_3/(Na_2O + K_2O) - Al_2O_3/(CaO + Na_2O + K_2O)$ [44] ratios, all rocks of the Medvedev massif correspond to rocks that form from a parent magma chamber of the oceanic crust (Figure 6A,B). According to the discrimination diagram [45] (Figure 6C–E) as well as ASI $Al_2O_3/(CaO + Na_2O + K_2O) < 1.05$ (Table A1), the geodynamic setting of the magma forming phases of the Medvedev massif defines them as volcanic arcs [46], while the ratio Zr/Al_2O3-TiO_2/Al_2O_3 defines them as oceanic and continental arcs [47] (Figure 6F).

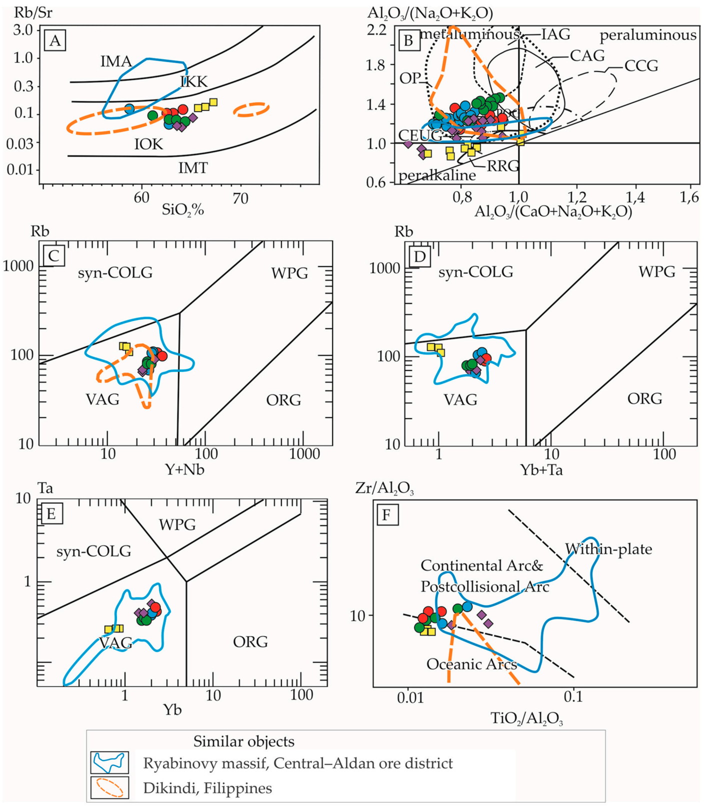

Figure 6. Discrimination diagrams for igneous rocks of the Medvedev, Taezhniy massifs and similar objects [10,24]. Blue line color is Ryabinovy massif, Central–Aldan ore district [14], Red line color is Dikindi, Fil-ippines [1]. (**A**) Rb/Sr-SiO_2diagram fields [43], igneous rocks: IMT—tholeiitic rock series, IKK—continental crust, IOK—oceanic crust, IMA—alkaline mantle; (**B**) $Al_2O_3/(Na_2O + K_2O) - Al_2O_3/(CaO + Na_2O + K_2O)$ diagram fields [46]: IAG—island arc granitoids, CAG—granitoids of continental arcs, CCG—granitoids of continental collision settings, POG—postorogenic granitoids, RRG—rift-related granitoids, CEUG—granitoids of continental epiorogenic uplifts, OP—oceanic plagiogranites; (**C**–**E**) Rb − Y + Nb, Rb − Tb + Ta, Ta − Yb diagram fields [45]: ORG—granites of oceanic ridges, WPG—intraplate granites, VAG—granites of volcanic arcs, syn-COLG—collision granites; (**F**) Zr/Al_2O_3 − TiO_2/Al_2O_3 diagram for various geodynamic settings according to [47]: WIP—intraplate rocks, CAP + PAP – marginal—continental and post-collision volcanic arcs, OAR—oceanic arcs. The other symbols are same as in Figure 4.

The ratio Sr-Rb/Sr [48] corresponds with the trend of differentiation in volcanic series of continental rift zones (Figure 7A). The parameters of the primary strontium isotope ratio I_0 = 0.708 (Table A5) for the first phase of the intrusion of Medvedev massif are typical for mid-ocean ridge basalts and some volcanic ocean islands with a lower crust source [49]. It is noteworthy that this parameter decreases from earlier leucocratic to later rocks of the massif.

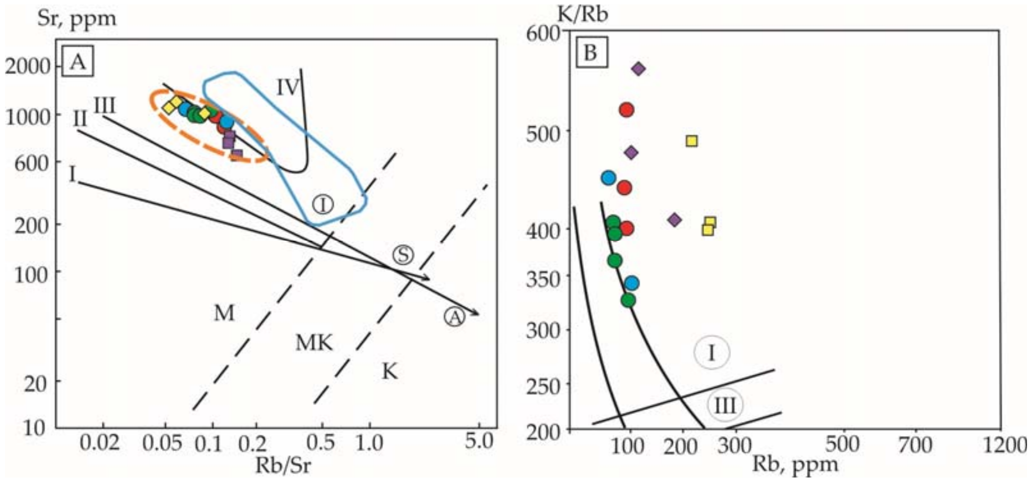

Figure 7. (**A**) Sr-Rb/Sr ratio in igneous rocks from Medvedev and Taezhniy massifs. Composition fields of magma-forming sources [48]: M—mantle, MK—mantle-crustal, K—crustal; 1—typical compositions of M, I, S and A-type granites; 2—trends of differentiation of type and volcanic series: I—tholetic of island arcs (OD), II—calc-alkaline (CA), III—calc-alkaline of active continental margins (ACM); IV—rift zones of the continents; (**B**) K/Rb-Rb ratio in igneous rocks: diagram fields according to [50], formations: I—mantle, III—mantle-crustal. The plots were performed according to the ICP MS data. The other symbols and fields are as in Figures 4 and 6, respectively.

The ratios of K/Rb = 175.98–290.30, Ba/Rb = 12.28–36.26, Rb/Sr = 0.10–0.12 (Table A2) and K/Rb-Rb, Sr-Rb/Sr (Figures 6 and 7) in *quartz syenites* of the first phase of Medvedev massif are characteristic to rocks formed from a mantle source [48,50]. The Nb/La = 0.25–0.27 ratio, as well as Th/U within the range of 3.20–3.93 (Table A3), shows the degree of magma contamination by continental crust [51,52]. A high Y/Nb = 2.33–2.43 > 1.2 ratio (Table A3) (in general, for all rocks of the massif) may indicate the contribution of both crustal and mantle sources [53]. The first phase rocks are characterized by a weak negative Eu-anomaly Eu/Eu* = 0.90–0.91 (Table A3), which may suggest the formation from primary mantle magmas during the fractional crystallization of dark-colored rock-forming minerals [53].

The ratios of K/Rb = 171.41–229,58, Ba/Rb = 4.81–29.63, Rb/Sr up to 0.12 (Table A2) and K/Rb-Rb, Sr-Rb/Sr (Figures 6 and 7) in *second phase syenites* of the massif correspond to mantle rocks [48,50]. Whereas the parameters of the primary ratio of strontium isotopes I_0 = 0.707 (Table A5) are for the rocks of the second stage of intrusion of the Medvedev massif, it is typical for rocks with a lower crustal source [49]. The values of Nb/La = 0.23–0.30 and Th/U = 4.31–5.89 (Table A3) may indicate the crust contamination of primary mantle magmas [52,54]. A significant increase in the ratio Eu/Eu* for 0.92–0.95 is close or equivalent to chondrite and indicates melt formation during fractional crystallization of only dark-colored rock-forming minerals. It also suggests deep differentiation [53].

The ratios of K/Rb = 179.95–251.62, Ba/Rb = 18.52–27.78, Rb/Sr ratios up to 0.1 (Table A2), K/Rb-Rb ratios and Sr-Rb/Sr (Figures 6 and 7) in *quartz monzonites* of the third phase of the Medvedev massif have mantle marks [48,50]. On the contrary, the parameters of the primary ratio of strontium isotopes I_0 = 0.706 (Table A5) are typical for rocks formed from a lower crustal source [49]. Low values of Nb/La = 0.24–0.33, as well as high values of Th/U = 3.69–4.43 in quartz monzonites (Table A3), as well as in other rocks of the massif, may indicate the crust contamination of primary magmas [52,54]. Relative europium content Eu/Eu* 0.88–0.95 is close to the mantle [53], which may also indicate melt formation during fractional crystallization of only dark-colored rock-forming minerals, suggesting deep differentiation [53].

According to the Rb/Sr-SiO_2 ratios [43], the rocks of the Taezhniy massif correspond to formations from parent magma chambers of the oceanic crust. According to the ratio Al_2O_3/(Na_2O + K_2O) − Al_2O_3/(CaO + Na_2O + K_2O) [44], the rocks of the first phase belong to oceanic plagiogranites, while the rocks of the second phase are related to rifts. The geodynamic position the same as for the rocks of the Medvedev massif, determined by the discrimination diagrams [45] (Figure 6), and the ASI Al_2O_3/(CaO + Na_2O + K_2O) < 1.05, defines them as formations of volcanic arcs. The ratio Zr/Al_2O_3-TiO_2/Al_2O_3 attributed them to oceanic and continental arcs [47] (Figure 6F). The Sr-Rb/Sr ratio [48] corresponds to the trend of differentiation of volcanic series in the rift zones of the continents (Figure 7A).

The ratios of K/Rb = 271.13–559.74, Ba/Rb up to 30.56 and Rb/Sr = 0.06–0.09 (Table A2) and the ratios K/Rb – Rb and Sr – Rb/Sr (Figure 7A,B) in *quartz monzonites* of the Taezhniy massif are characteristic to rocks formed from a mantle source [48,50]. The parameters of the primary ratio of strontium isotopes I_0 = 0.706 (Table A5) are typical for rocks formed from a lower crustal source [49]. Low values of Nb/La = 0.27–0.32, as well as values of Th/U = 2.19–2.66 the rocks of the phase (Table A3) may indicate magma crust contamination [52,54]. High Y/Nb = 2.31–2.43 (Table A3) may indicate the contribution of both crustal and mantle sources [53]. The rocks of the massif phases are characterized by the presence of a weak negative Eu-anomaly Eu/Eu* = 0.88–0.91, which may indicate the formation of the parent melt during the fractional crystallization of dark-colored rock-forming minerals [53].

The values of ratios K/Rb = 359–734.3, Ba/Rb up to 23, Rb/Sr = 0.13–0.16 (Table A2) and ratios K/Rb – Rb, Sr – Rb /Sr (Figure 7A,B) in *syenites* of the second phase of the massif correspond to mantle rocks [48,50]. The parameters of the primary ratio of strontium isotopes I_0 = 0.707 (Table A5) for the rocks of the second stage of intrusion of the Taezhniy massif are typical for rocks with a lower crustal source [49]. The values of Nb/La = 0.42–0.51 and Th/U = 3.66–4.69 (Table A3) may suggest the crust contamination of primary mantle magmas [52,54]. A significantly higher relative content of europium Eu/Eu* = 0.85–0.95 compared to rocks of the previous phase is close to mantle [53]. It may also indicate melt formation during the fractional crystallization of only dark-colored rock-forming minerals and point to deep differentiation [53].

5. Discussion

5.1. Petrography of Rocks of Medvedev Massif

The three phases of intrusion of rocks with distinctive contacts between the latter, differing in composition and structure were identified for the first time at expedition work and the crystal optical studies of igneous rocks of the Medvedev massif: I phase quartz syenites, II phase pyroxene-amphibole syenites and III phase quartz monzonites.

5.2. Geochemical Composition of Rocks of Medvedev Massif

According to geochemical composition next groups of rocks defined in Medvedev massif: quartz syenites (I phase), syenites (II phase) of shoshonite series and quartz monzonites (III phase) of high potassium calc-alkaline petrochemical series. The first and second phase rocks of Medvedev massif (as almost all studied rocks) belonging to the shoshonite series has important metallogeny significance, since that series is sometimes associated with various types of mineralization: industrial molybdenum, polymetallic, gold-polymetallic and gold mineralization, as well as occurrences of arsenic, antimony and other metals [8,55–59].

The total content of alkalis (Na_2O + K_2O) < 12 in the igneous formations of the Medvedev massif corresponds to subalkaline rocks (I) 8.15%–11.88%, (II) 7.72%–9.69% and (III) 7.87%–8.89%. The quartz syenites of the Medvedev massif are characterized by potassium type of alkalinity Na_2O/K_2O < 1, while for syenites of the second phase, this indicator is intermediate Na_2O/K_2O 0.85–1.17 (mostly corresponds to the conditions

$Na_2O/K_2O > 1$), and in monzonites, the parameter $Na_2O/K_2O > 1$ corresponds to the rocks of the potassium–sodium series of alkalinity. Decreases in the values of alumina in the rocks of the Medvedev massif from quartz syenites al′ = 1.15–2.69 to syenites of the second phase al′ = 0.37–2.06 with a subsequent increase in monzonites al′ = 1.12–2.98, and a noticeable decrease in the AG coefficient in this series from 0.74–0.86 to 0.68–0.80, along with petrographic studies, may reflect the sequence of rock intrusion.

The rocks of the Medvedev massif are geochemically specialized to Rb, Ba, Sr, B, Cr, V, Nb and Sc (Table A2), i.e., to lithophile elements. The content of chalcophile Cu, Sn, Zn, Pb, Ge and siderophile Ni and Co elements is significantly lower. These indicators differ in the contents in phases of the massif. High content in all rocks of massif Rb, Ba, Sr, Zr, Nb and Co correspond to the latite series. REE distribution with smooth negative incline shows the enrichment of cerium (La, Ce, Nd, Pr, Sm, Eu) and a depletion of yttrium (Y, Gd, Tb, Dy, Ho, Er, Tm, Yb, Lu) elements. It is worth noting that the highest concentration of REE in quartz syenites ∑REE 180.77 decreases to monzonites ∑114.01.

5.3. Geochronology of Rocks of Medvedev Massif

The concordant period of the evolution of the Medvedev massif, dated by the SHRIMP 2 method, is 122.0–118.0 Ma, which corresponds quite well with geological observations.

5.4. Formation Conditions of Rocks of Medvedev Massif

Opinions vary on the role of subducted oceanic crust of the Mongol–Okhotsk Ocean in the formation of parent magma chambers of the Aldan Mesozoic igneous complex [15,17,60–62]. The potassium alkaline Mesozoic magmatism of the Aldan Shield is of interest in terms of the genesis of intratelluric magmas and their ore content [15,60,62,63].

E.P. Maximov et al. [15,60] suggested that the subducted oceanic crust of the Mongol–Okhotsk Ocean participated in the formation of all parent magma chambers of the Aldan Complex. This point of view is shared by A.Y. Kochetkov and Lazebnik [61], who emphasized the geochemical affinity of Mesozoic magmatic formations to the vulcanites of island arcs. V.A. Kononova et al. [62] hold a different viewpoint based on the geochemical analysis of potassium rocks of Central Aldan and certain similarities between them and volcanic products of continental margin and island arcs (Italy, Indonesia) [62] and their distinction from rocks of ancient platforms (Africa) [62]. The geochemical data obtained for Mesozoic igneous rocks of the Evotinskiy ore district by and large support this position.

The ratios of Rb/Sr-SiO_2 and $Al_2O_3/(Na_2O + K_2O) - Al_2O_3/(CaO + Na_2O + K_2O)$ of all rocks of the Medvedev massif show their formation from a parent magmatic chamber of the oceanic crust (Figure 6A,B) [43,44].According to the discrimination diagram [45] (Figure 6C–E), ASI $Al_2O_3/(CaO + Na_2O + K_2O) < 1{,}05$ (Table A1), and the ratios of Zr/Al_2O_3-TiO_2/Al_2O_3, Sr-Rb/Sr the geodynamic setting of the magma forming phase defines the analyzed igneous rocks as volcanic arcs [45–48] (Figures 6F and 7A). Similar conclusions were made for the similar igneous formations of the Central Aldan ore district [24,62], northern Luzon (Philippines) [10], northern China, etc. [11,64] (Figure 6). All mentioned areas show a similar geodynamic setting and the genesis of subalkaline and alkaline rocks.

The ratios of K/Rb, Rb/Sr and Ba/Rb and K/Rb-Rb and Sr-Rb/Sr elements designate all rocks of the Medvedev massif as close to mantle rocks. A high ratio of $Y/Nb > 1.2$ may, in general, indicate the contribution of both crustal and mantle sources. A lower crust source is attested by the ratios of Sr primary isotopes $I_0 = 0.706$–0.708 (Table A5) [49] as well as low values of $Nb/La < 1$ characteristic for all analyzed rocks that indicate a negative niobium (tantalum) anomaly and high values of $Th/U > 2$ as a an apparent sign of crust contamination [52,54]. In contrast, the relative content of europium $Eu/Eu^{*} \approx 1$ suggests that the rocks of the massif are close to mantle and that melt formed during fractional crystallization of only dark-colored rock-forming minerals [53].

It should be noted that the increased values of the elemental U/Th ratio from the first to the third phase, with maximum values in the second phase of the Medvedev massif, and some chalcophile elements may also indicate an increased filling fluids in the rocks [65]. The latter is apparently associated with degassing of the second and third phases of the massif followed by the circulation of fluids in the system [20,66], which can also be indicated by a decrease in pressure during the crystallization of pyroxenes from the first phase to the last one [67], degassing can be indirectly confirmed by the presence of miarols in the rocks of the second and third phases.

5.5. Petrography of Rocks of Taezhniy Massif

In the Taezhny massif during field and crystal-optical studies, a two-phase structure was identified for the first time: phase I quartz monzonites and phase II syenites.

5.6. Geochemical Composition of Rocks of Taezhniy Massif

According to geochemical composition next groups of rocks defined in Taezhniy massif: quartz monzonites (phase I) with ambiguous geochemical characteristics, in which they are close to both high-potassium calc-alkaline and shoshonite petrochemical series, and syenites (phase II) of the shoshonite petrochemical series.

The total content of alkalis ($Na_2O + K_2O$) < 12 in the igneous formations of the Taezhny massif correspond to subalkaline rocks: the first phase is 8.64%–10.35% and the rocks of the second phase are 10%–13.67%. All rocks of the Taezhniy massif are characterized by the potassium type of alkalinity $Na_2O/K_2O < 1$.

Geochemically, the rocks of the Taezhniy massif are specialized for the same number of elements as the rocks of the Medvedev massif, i.e., both for lithophile Rb, Ba, Sr, B, Cr, V, Nb and Sc (Table A2) and for chalcophile Cu, Sn, Zn Pb and Ge. These indicators differ in massif phases. High contents of Rb, Ba, Sr, Rb, Zr, Nb and Co correspond to the rocks of the latite series. The pattern of REE distribution in the rocks of the Taezhniy massif is similar to the rocks of the Medvedev massif, i.e., they are enriched in cerium (La, Ce, Pr, Nd, Sm, Eu) and depleted in yttrium (Y, Gd, Tb, Dy, Ho, Er, Tm, Yb, Lu) elements. The decreasing of amount of $\sum$REE from 177.95 to 66.89 in the rocks of the Taezhniy massif may indicate a normal differentiation course. The ratios La/Yb and Ce/Yb in all rocks of the massif are close to those of the latite series.

5.7. Geochronology of Rocks of Taezhniy Massif

The dating of rocks of the Taezhniy massif is not quite clear. The rocks of the first phase (quartz monzonites) dated by the SHRIMP 2 method are younger, with a mark of a concordant age of 117.5 $\pm$ 1.5 Ma, while the rocks of the second phase (syenite), which were later geologically observed, have a concordant age of 120.8 $\pm$ 2.6 Ma. As previously noted, the presence of older points in zircons is probably associated with the presence of quartz monzonite xenoliths in these rocks, the zircons from which were dated and taken into account when compiling Concordia. The obtained minimum age value of 114.5 $\pm$ 1.9 Ma for zircons from rocks of the second phase (syenites) is the closest to reality, while in the rocks of the first phase (quartz monzonites) this parameter is 115.6 $\pm$ 1.8 Ma. Thus, the formation interval of rocks of the Taezhniy massif should be accepted within 117.5–114.5 Ma.

5.8. Formation Conditions of Rocks of Taezhniy Massif

The geodynamic setting that existed during the formation of the rocks of the Taezhniy massif is similar to those of the Medvedev massif—defining them as the formation of volcanic arcs [45–48] (Figures 6F and 7A). The dual nature of the geochemical composition of massif rocks perhaps shows both the presence of crust and mantle sources. According to the K/Rb, Rb/Sr and Ba/Rb ratios and the K/Rb-Rb and Sr-Rb/Sr ratios of the elements, all the rocks of the Taezhniy massif are close to rocks of a mantle nature. A high Y/Nb > 1.2 ratio may indicate the contribution of both crustal and mantle sources. A lower crust source is attested by the ratios of Sr primary isotopes I_0 = 0.706–0.707 (Table A5) [49] as well as low values of the Nb/La < 1 characteristic, which indicates a negative niobium (tantalum) anomaly and high values of Th/U >2 as a an apparent sign of crust contamination [52,54]. In contrast, the relative content of europium Eu/Eu*≈1 suggests that the rocks of the massif are close to mantle derivates and that the melt formed during the fractional crystallization of only dark-colored rock-forming minerals [53].

6. Conclusions

The presented work is the final stage of many years of field and analytical work. The authors are the first who performed petrographic, geochemical, isotope and geochronological studies of the Medvedev and Taezhniy massifs and came to the following conclusions:

1. According to field, petrographic and geochemical observations, it was revealed that the formation of the Medvedev massif occurred in three phases of rock intrusion and are presented in the following sequence: quartz syenites, pyroxene-amphibole syenites, quartz monzonites. According to the results of the same studies, two phases of rocks are defined in the structure of the Taezhniy massif: quartz monzonites and syenites.
2. In terms of geochemical characteristics, the igneous formations of the Medvedev and Taezhniy massifs are similar to rocks derived from the latite and shoshonite series and can be considered as part of the monzonite–syenite formation type.
3. The periods of formation of igneous rocks of the massifs were identified (Medvedev—122.0–118.0 Ma and Taezhniy—117.5–114.5 Ma) which correspond to the Early Cretaceous age of the Aptian.
4. The opinion expressed previously regarding the participation of the subducted oceanic crust of the Mongolian–Okhotsk basin in the formation of all parent igneous chambers of the Aldan Complex, as well as the geochemical proximity of the rocks of the Mesozoic igneous formations with island arc volcanics, in general, is confirmed by our obtained geochemical data of the rocks of the Medvedev and Taezhniy massifs.
5. The defined duality of the geochemical compositions of the igneous rocks of the massifs may be due to the presence of both mantle and crustal sources; however, it is most likely that these rocks resulted from the melting of a mixed mantle source or the latter contaminated by the crust with further the differentiation of melts in intermediate crust chambers.

Author Contributions: Conceptualization: A.I., E.L., M.I. and A.Z.; methodology, A.I., E.L., M.I. and A.Z.; validation, A.I., E.L. and A.Z.; formal analysis, A.I.; writing—original draft preparation, A.I., E.L., M.I. and A.Z.; writing—review and editing, A.I., E.L., M.I. and A.Z.; visualization, A.I., E.L., M.I. and A.Z.; supervision, A.I.; project administration, A.I.; funding acquisition, A.I., E.L., M.I. and A.Z. All authors have read and agreed to the published version of the manuscript.

Funding: Work is done on state assignment of DPMGI SB RAS and partially funded by contract with PJSC Seligdar.

Data Availability Statement: Not applicable.

Conflicts of Interest: The authors declare no conflict of interest.

Appendix A

Table A1. Geochemical composition of the igneous rocks of Medvedev and Taezhniy massifs (all values in %; nd—not detected).

Sample	Massif	Phase	SiO_2	TiO_2	Al_2O_3	Fe_2O_3	FeO	MnO	MgO	CaO	Na_2O	K_2O	H_2O^-	H_2O^+	P_2O_5	CO_2	S	F	Total	Na + K	Na/K	al′	AG	ASI
I19–19/3	Medvedev	1	61.55	0.56	15.74	3.39	2.56	0.13	2.09	4.44	4.24	4.35	0.20	0.03	0.36	0.27	nd	0.04	99.95	8.59	0.97	1.42	0.74	0.80
I19–19/4			63.61	0.53	17.00	2.01	2.28	0.13	0.83	3.32	4.38	5.20	0.36	0.15	0.18	0.49	nd	0.03	100.50	9.58	0.84	2.57	0.75	0.90
I19–19/6			63.69	0.48	17.40	1.83	2.37	0.12	2.36	0.43	4.62	5.98	0.40	0.45	0.17	0.11	0.01	0.04	100.46	10.60	0.77	1.66	0.81	1.17
I19–19/7			63.68	0.53	16.63	3.03	1.87	0.09	1.02	2.45	4.59	5.12	0.58	0.32	0.18	0.27	nd	0.10	100.46	9.71	0.90	2.32	0.79	0.95
I19–19 2			61.41	0.24	16.30	2.25	1.68	0.08	4.08	2.51	4.52	5.32	0.40	0.69	0.17	0.86	nd	0.03	100.54	9.84	0.85	1.15	0.81	0.92
I19–22			63.50	0.52	16.34	2.45	1.81	0.09	0.87	2.87	4.69	5.32	0.34	0.51	0.20	nd	nd	0.05	99.56	10.01	0.88	2.58	0.82	0.87
I19–22/2			63.73	0.49	16.57	2.84	1.68	0.08	0.82	2.78	4.83	5.42	0.40	0.05	0.18	0.05	nd	0.05	99.97	10.25	0.89	2.64	0.83	0.88
I19–22/3			63.21	0.43	16.72	2.35	2.01	0.06	1.05	2.32	3.80	6.59	0.52	0.23	0.17	0.27	0.01	0.05	99.79	10.39	0.58	2.39	0.80	0.95
I19–22/4			64.00	0.41	16.56	2.35	1.86	0.10	0.80	3.04	4.96	5.12	0.38	nd	0.21	0.22	nd	0.05	100.06	10.08	0.97	2.69	0.83	0.86
I19–22/5			62.57	0.46	16.49	2.13	2.23	0.09	0.89	3.42	5.29	5.04	0.34	0.06	0.18	0.38	nd	0.06	99.63	10.33	1.05	2.44	0.86	0.81
I19–9		2	63.06	0.51	16.41	2.27	2.62	0.13	1.10	3.59	4.38	4.42	0.48	0.88	0.33	0.53	0.02	0.08	100.81	8.80	0.99	2.06	0.73	0.89
M18–6			62.8	0.55	15.74	2.41	2.60	0.13	1.56	4.06	4.64	3.95	0.28	0.40	0.33	0.14	nd	0.06	99.65	8.59	1.17	0.37	0.75	0.86
I19–9/3			60.17	0.53	15.28	3.32	2.06	0.11	1.42	3.47	4.25	4.13	0.22	1.69	0.39	2.65	0.01	0.08	99.78	8.38	1.03	1.42	0.71	0.89
I19–9/5			61.20	0.62	15.27	3.65	2.73	0.12	1.86	3.34	3.77	4.45	0.58	1.28	0.45	1.03	nd	0.10	100.45	8.22	0.85	1.46	0.79	0.77
I19–9/6			60.15	0.59	15.20	3.49	2.77	0.14	1.68	4.26	4.43	4.36	0.56	1.18	0.44	1.45	nd	0.08	100.78	8.79	1.02	1.40	0.83	0.74
I19–9/7			60.11	0.61	15.35	3.66	2.69	0.15	1.92	4.48	4.49	4.91	0.24	0.27	0.53	0.40	nd	0.10	99.91	9.40	0.91	1.44	0.82	0.72
I19–10			59.97	0.78	15.21	3.82	2.59	0.15	1.77	4.71	4.49	4.71	0.34	0.22	0.53	0.33	nd	0.10	99.72	9.20	0.95	1.68	0.79	0.76
I19–11			60.28	0.66	15.68	4.06	2.36	0.16	1.34	4.54	4.50	4.66	0.40	0.46	0.48	0.38	nd	0.08	100.04	9.16	0.97	1.59	0.79	0.76
I19–11/2			61.29	0.67	15.49	4.12	2.01	0.14	1.69	4.48	4.52	4.40	0.30	0.42	0.48	0.63	0.02	0.08	100.74	8.92	1.03	1.65	0.80	0.84
I19–11/4			61.58	0.57	15.82	3.73	2.05	0.16	1.70	3.42	4.78	4.44	0.54	0.70	0.51	0.59	0.03	0.08	100.70	9.22	1.08	1.40	0.81	0.81
I19–11/5			61.51	0.63	15.67	3.71	2.33	0.13	2.19	3.66	4.68	4.56	0.34	0.25	0.48	0.57	0.01	0.09	100.81	9.24	1.03	1.49	0.84	0.77
I19–11/6			61.92	0.63	15.15	3.75	2.47	0.12	1.68	3.92	4.72	4.53	0.34	0.34	0.47	0.56	0.01	0.09	100.70	9.25	1.04	1.38	0.78	0.82
I19–12			61.54	0.62	15.54	3.52	2.29	0.14	2.29	3.79	4.48	4.36	0.48	0.33	0.44	0.58	nd	0.09	100.49	8.84	1.03	1.24	0.76	0.80
I19–21/2			60.47	0.73	15.48	3.99	2.72	0.13	2.39	4.12	4.14	4.56	0.38	0.78	0.37	0.16	nd	0.03	100.45	8.70	0.91	1.42	0.72	0.83
I19–21/3			60.44	0.74	15.90	4.18	2.30	0.11	2.09	4.25	4.02	4.46	0.54	0.86	0.39	0.32	nd	0.04	100.64	8.48	0.90	1.06	0.84	0.73
I19–21/5			58.81	0.69	14.81	3.62	3.41	0.13	2.68	4.26	4.45	4.77	0.34	0.54	0.57	0.22	0.03	0.1	99.43	9.22	0.93	1.72	0.76	0.82
I19–7		3	64.43	0.47	16.43	2.09	2.29	0.12	0.88	3.49	4.89	3.93	0.34	0.22	0.24	0.21	nd	0.08	100.11	8.82	1.24	2.41	0.75	0.88
I19–13			62.77	0.58	15.20	2.88	3.39	0.10	1.75	3.27	4.96	3.71	0.30	0.39	0.44	0.59	nd	0.09	100.42	8.67	1.34	1.37	0.80	0.84
I19–14			63.14	0.55	16.39	2.64	2.49	0.09	1.37	3.75	4.56	4.01	0.36	0.40	0.26	0.11	0.01	0.01	100.14	8.57	1.14	1.89	0.72	0.88
I19–15			63.56	0.45	16.68	2.65	1.96	0.10	1.22	3.55	4.61	3.99	0.26	0.55	0.24	0.17	nd	0.02	100.01	8.60	1.16	2.21	0.71	0.91
I19–16			64.10	0.44	16.81	4.54	0.21	0.09	0.97	3.78	4.57	3.90	0.20	0.24	0.22	nd	0.01	0.03	100.11	8.47	1.17	2.98	0.70	0.90
I19–17			62.90	0.51	16.53	2.32	2.79	0.10	1.36	3.58	4.71	3.80	0.30	0.33	0.28	0.11	nd	0.03	99.65	8.51	1.24	1.86	0.72	0.90
I19–18			65.41	0.28	15.72	1.56	0.99	0.08	0.05	2.47	4.97	6.23	0.22	0.44	0.11	1.37	0.01	0.02	99.93	11.20	0.80	1.12	0.68	0.94

Table A1. *Cont.*

Sample	Massif	Phase	SiO_2	TiO_2	Al_2O_3	Fe_2O_3	FeO	MnO	MgO	CaO	Na_2O	K_2O	H_2O^-	H_2O^+	P_2O_5	CO_2	S	F	Total	Na + K	Na/K	al′	AG	ASI
I19–20			62.00	0.53	16.22	2.13	3.30	0.12	3.33	3.47	4.41	3.46	0.28	0.41	0.30	0.44	nd	0.03	100.43	7.87	1.27	1.41	0.71	0.86
I19–20/2			62.79	0.40	16.27	1.54	3.21	0.13	2.39	4.06	4.61	3.59	0.30	0.20	0.30	0.70	nd	0.03	100.52	8.20	1.28	1.64	0.70	0.87
I19–20/3			63.27	0.46	16.54	1.32	3.24	0.13	1.85	4.04	4.68	3.63	0.28	0.05	0.26	0.49	nd	0.03	100.27	8.31	1.29	2.08	0.72	0.89
I19–20/4			63.66	0.44	16.43	2.13	2.16	0.12	1.37	3.61	4.68	3.80	0.34	0.49	0.22	0.16	0.01	0.03	99.65	8.48	1.23	1.79	0.71	0.86
I19–20/5			63.08	0.55	16.03	2.39	2.27	0.10	1.66	3.94	4.34	3.98	0.56	0.31	0.25	0.38	0.02	0.03	99.89	8.32	1.09	2.24	0.72	0.91
I19–21/6			62.85	0.44	16.67	2.72	1.99	0.10	1.14	3.43	4.72	3.98	0.50	0.40	0.26	nd	nd	0.08	99.28	8.70	1.19	2.35	0.69	0.92
I19–21/7			63.85	0.40	16.33	2.37	1.87	0.09	1.11	3.60	4.30	3.80	0.68	0.31	0.26	nd	nd	0.05	99.02	8.10	1.13	2.44	0.74	0.90
I19–21/8			64.04	0.38	16.74	2.45	1.95	0.09	1.00	3.36	4.99	3.90	0.28	0.22	0.27	0.05	nd	0.05	99.77	8.89	1.28	1.12	0.68	0.75
I19–24/2	Taezhniy	1	63.97	0.36	16.14	2.87	1.26	0.08	1.21	3.53	5.53	3.79	0.12	0.20	0.23	0.27	nd	0.08	99.67	9.32	1.46	2.42	0.82	0.82
I19–24/4			63.54	0.30	16.33	2.47	1.29	0.03	1.22	3.56	5.56	4.72	0.32	nd	0.24	0.17	nd	0.05	99.8	10.28	1.18	2.51	0.87	0.79
I19–26			63.92	0.42	15.93	2.62	1.37	0.07	1.15	2.8	6.15	4.79	0.14	0.03	0.24	0.27	0.01	0.05	99.96	10.94	1.28	2.44	0.96	0.78
I19–26/2			63.29	0.34	16.13	2.64	1.29	0.08	1.23	3.62	5.65	4.61	0.22	0.22	0.24	0.27	nd	0.08	99.91	10.26	1.23	2.43	0.89	0.77
I19–26/3			62.17	0.48	13.88	1.85	2.67	0.05	2.46	3.51	4.18	7.29	0.16	0.04	0.44	0.16	nd	0.08	99.42	11.47	0.57	1.24	1.06	0.66
I19–26/4			66.00	0.31	15.74	2.03	0.99	0.06	0.97	2.29	4.71	5.75	0.26	nd	0.19	0.28	nd	0.05	99.64	10.46	0.82	3.06	0.89	0.87
I19–26/5			59.71	0.57	14.03	3.23	2.15	0.09	2.86	4.75	3.93	7.12	0.24	nd	0.50	0.44	0.02	0.12	99.76	11.05	0.55	1.14	1.01	0.62
I19–29			62.28	0.52	15.03	3.19	1.65	0.11	1.06	2.91	5.61	7.22	0.26	0.04	0.24	0.34	0.03	0.09	100.58	12.83	0.78	2.13	1.13	0.67
I19–29/2			61.24	0.53	16.00	3.50	2.11	0.11	1.18	3.68	5.10	5.37	0.46	0.28	0.28	0.55	0.01	0.01	100.41	10.47	0.95	1.95	0.89	0.77
I19–29/4			65.06	0.20	16.47	1.68	1.00	0.06	0.61	1.74	5.49	6.19	0.10	0.27	0.09	0.52	0.01	0.03	99.52	11.68	0.89	4.09	0.95	0.87
I19–29/5			66.78	0.22	16.25	1.39	1.15	0.05	0.56	1.17	5.20	nd	0.30	0.21	0.06	0.25	0.01	0.01	99.73	11.32	0.85	4.13	0.93	0.94
I19–30/2			64.42	0.44	16.38	2.69	1.43	0.06	0.79	2.83	4.95	4.59	0.32	0.26	0.20	0.25	nd	0.01	99.62	9.54	1.08	2.85	0.80	0.90
I19–30/3			65.14	0.45	15.92	2.53	1.37	0.06	0.84	2.91	4.82	4.63	0.18	0.21	0.21	0.33	nd	0.04	99.64	9.45	1.04	2.8	0.81	0.87
I19–30/4			64.90	0.41	15.37	2.90	1.66	0.06	1.14	2.63	4.76	5.04	0.30	0.28	0.31	0.4	0.01	0.06	100.23	9.80	0.94	2.17	0.86	0.85
I19–30/5			61.91	0.47	15.96	2.18	3.75	0.09	1.02	3.50	4.80	4.43	0.30	0.05	0.26	0.58	0.02	0.07	99.39	9.23	1.08	1.72	0.79	0.84
I19–27/2		2	67.48	0.19	15.97	1.68	1.00	0.05	0.75	1.85	5.09	4.91	0.26	0.14	0.13	0.49	0.02	0.05	100.06	10.00	1.04	3.64	0.86	0.94
I19–27/4			67.69	0.14	16.06	1.75	0.70	0.04	0.80	0.66	5.61	5.06	0.28	0.13	0.13	0.55	nd	0.04	99.68	10.67	1.11	3.89	1.00	1.01
I19–27/5			66.43	0.22	15.85	2.67	0.17	0.08	0.33	1.74	5.94	5.90	0.08	0.42	0.12	0.14	0.02	0.01	100.12	11.84	1.01	3.89	0.92	0.82
T19–27/6			67.22	0.20	15.82	1.21	1.39	0.05	0.24	1.13	6.00	6.12	0.58	0.34	0.11	0.29	0.01	0.01	100.72	12.12	0.98	5.70	1.02	0.85
I19–27/7			65.66	0.20	15.63	1.88	1.00	0.09	0.42	1.91	6.28	6.33	0.26	0.01	0.13	0.11	0.02	0.01	99.95	12.61	0.99	4.73	1.04	0.76
I19–28			64.71	0.14	16.50	1.22	1.11	0.06	0.57	1.64	6.25	6.59	0.10	0.32	0.07	0.18	nd	0.01	99.47	12.84	0.95	4.24	1.10	0.81
I19–28/2			66.26	0.18	16.23	1.68	0.57	0.06	0.40	0.83	5.75	7.86	0.26	0.18	0.06	0.28	nd	0.09	100.69	13.61	0.73	4.35	1.06	0.83
I19–28/3			62.32	0.44	15.45	2.86	1.41	0.10	0.92	2.91	5.83	7.2	0.18	0.31	0.20	0.17	0.01	0.04	100.35	13.03	0.81	5.63	1.11	0.68
I19–28/4			66.05	0.20	15.35	1.42	1.23	0.06	0.50	1.27	5.55	8.12	0.18	0.08	0.07	0.24	nd	0.03	100.35	13.67	0.68	2.51	1.12	0.76

* al′ =A l/(2Ca + Na + K); AG = $(Na_2O + K_2O)/Al_2O_3$; ASI = $Al_2O_3/(CaO + Na_2O + K_2O)$.

Table A2. Geochemical composition of the igneous rocks of Medvedev and Taezhniy massifs (all values in ppm; bdl—below detection limit).

Sample	Massif	Phase	Cu	Sn	Zn	Pb	Ge	Cr	V	Sc	Ba	Sr	Rb	Nb	Zr	B	Ni	Co	K/Rb	Rb/Sr	Ba/Rb
I19–19/3	Medvedev	1	9.02	bdl	100	39.2	bdl	71.6	88	8.35	1260	870	102.6	11.5	200	8.8	11.2	5.3	175.98	0.12	12.28
I19–19/4			8.27	bdl	61.5	48.9	bdl	160	84.2	7.93	1780	990	107.1	8.44	210	7.92	11.3	5.1	201.53	0.11	16.62
I19–19/6			81.9	bdl	53.2	32.2	bdl	300	89	7.83	3100	770	85.5	5.22	140	bdl	23.3	4.96	290.31	0.11	36.26
I19–19/7			21.6	bdl	60.8	49.4	bdl	110	99.1	9.16	2030	840	104.4	8.52	170	8.28	8.64	5.62	203.56	0.12	19.44
I19–19 12			7.54	bdl	bdl	40.7	bdl	140	77.3	8.12	2000	780	87.3	7.24	130	bdl	10.5	4.51	252.94	0.11	22.91
I19–22			14.9	bdl	73	21.2	bdl	110	94.1	10.3	1700	760	89.1	9.3	110	bdl	11.9	6.54	247.83	0.12	19.08
I19–22/2			21.4	bdl	bdl	20.8	bdl	25.4	89.1	8.67	2000	820	89.1	8.69	140	bdl	8.31	6.35	252.49	0.11	22.45
I19–22/3			36.7	bdl	bdl	20.5	bdl	57.8	93.2	6.33	2600	1010	103.2	9	157	8.83	14	5.8	264.93	0.1	25.18
I19–22/4			5.63	bdl	67.6	27.8	bdl	31.5	96.6	7.8	2100	860	87.3	10.4	120	bdl	8.82	4.67	243.43	0.1	24.05
I19–22/5			6.03	bdl	−58	22.4	bdl	29	93.3	7.27	2300	1000	103	9.9	171	bdl	8.57	5.62	203.02	0.1	22.32
I19–9		2	18.6	bdl	51	31.7	bdl	380	120	16	2100	920	85.5	5.32	260	8.11	27.6	12.5	214.58	0.09	24.56
I19–9/3			bdl	bdl	77.6	13.8	bdl	40	93.2	13.3	1500	590	79.2	10.6	200	10.9	18	12.2	216.45	0.13	18.94
I19–9/5			8.09	bdl	56.3	15.4	bdl	320	120	17.4	1500	940	89.1	4.73	270	bdl	29.3	11.7	207.3	0.09	16.84
I19–9/6			30.3	bdl	70.9	31.3	bdl	260	97.7	15.4	1000	750	81.9	7.84	210	8.89	34.7	13.3	220.97	0.11	12.21
I19–9/7			16.5	bdl	77.7	32.8	bdl	69.3	130	18.5	2800	1000	94.5	7.97	180	6.16	26	18.1	215.66	0.09	29.63
I19–10			25.5	bdl	66.5	27.3	bdl	50.3	120	18.1	2200	1000	93.6	4.12	190	8.99	22.6	16.2	208.87	0.09	23.5
I19–11			27.9	bdl	95.3	54.8	bdl	200	140	16.7	2100	900	93.6	4.96	200	8.41	26.8	16.6	206.65	0.1	22.44
I19–11/2			25.7	bdl	67.6	22.8	bdl	110	130	18.2	1600	950	83.7	8.28	210	bdl	26.8	17.4	218.2	0.09	19.12
I19–11/4			15.5	bdl	68.3	20.2	bdl	44.9	110	15.8	1500	770	86.4	7.94	210	bdl	22.3	12.9	213.3	0.11	17.36
I19–11/5			82	bdl	99	25.5	bdl	152	120	16.5	2300	1000	85.5	9.52	180	bdl	24.1	15.5	221.37	0.09	26.9
I19–11/6			100	bdl	81.9	28.3	bdl	103	120	16.8	1600	870	81.9	3.66	140	bdl	20	14	229.58	0.09	19.54
I19–12			30.4	bdl	110	27.1	bdl	132	110	15.3	1700	820	82.8	3.94	170	10.1	21.5	13.8	218.57	0.1	20.53
I19–21/2			29.1	bdl	100	29.2	bdl	180	130	17.9	1700	900	101.7	8.73	170	bdl	29.9	15.4	186.11	0.11	16.72
I19–21/3			15.3	bdl	88.5	27.7	bdl	130	120	17.3	1600	890	108	7.57	210	bdl	23.8	14.1	171.41	0.12	14.81
I19–21/5			65	bdl	100	33.3	bdl	94	130	20.2	2000	917	113.4	6.8	220	bdl	35	20	174.65	0.12	17.64
M18–6			13.9	bdl	68.6	26	bdl	150	85.6	9.55	2120	1100	71.5	7.87	120	bdl	11.8	9.15	229.38	0.06	29.66
I19–7		3	9.44	bdl	68.9	30.7	bdl	27.6	63.8	8.39	1600	1030.2	78.9	10.1	150	bdl	9.54	7.42	206.81	0.08	20.29
I19–13			24.1	bdl	82.5	27	bdl	43.5	68.9	10.3	1700	850	61.2	7.65	150	8.54	13.6	9.07	251.62	0.07	27.78
I19–14			14.6	bdl	66	35.4	bdl	54.6	69.5	10.4	1700	1000	91.8	10.8	190	bdl	14	8.51	181.31	0.09	18.52
I19–15			10	bdl	bdl	26.1	bdl	47.6	66.1	9.03	1900	1030	82	8.6	170	bdl	11.8	6.71	201.92	0.08	23.16
I19–16			10.3	bdl	65.1	34.5	bdl	32.1	72.5	8.45	1800	1000	87.3	6.68	160	8.2	9.63	7.31	185.43	0.09	20.62
I19–17			17.4	bdl	71.5	29.6	bdl	110	73.5	9.84	2000	1000	73.8	6.39	160	8.88	14	7.93	213.72	0.07	27.1
I19–20			36.4	bdl	79.8	34	bdl	51.1	80.6	10.5	1600	780	66.6	9.35	150	bdl	12.2	10.1	215.64	0.09	24.02
I19–20/2			23.9	bdl	74.6	36.4	bdl	260	72.7	11.3	2000	1060	79.5	6.15	140	bdl	13.3	8.27	187.32	0.08	25.14
I19–20/3			19.4	bdl	64	28.4	bdl	61.1	66.7	9.73	1900	1000	77.4	5.32	130	bdl	11.9	8.99	194.67	0.08	24.55

Table A2. *Cont.*

Sample	Massif	Phase	Cu	Sn	Zn	Pb	Ge	Cr	V	Sc	Ba	Sr	Rb	Nb	Zr	B	Ni	Co	K/Rb	Rb/Sr	Ba/Rb
I19–20/4			10.5	bdl	57.8	25.7	bdl	36.1	64.4	8.36	1600	900	80.1	10.5	150	bdl	9.64	7.35	196.91	0.09	19.98
I19–20/5			17.8	bdl	78.7	32.2	bdl	36.5	65.1	7.86	1900	880	91.8	8.02	120	bdl	12.3	9.95	179.96	0.1	20.7
I19–21/6			17.3	bdl	61.7	35.8	bdl	110	74.7	8.92	1600	820	71.1	7.63	150	66.2	11.5	8.28	232.35	0.09	22.5
I19–21/7			41.9	bdl	82.2	26.8	bdl	27.6	66.9	8.92	1500	940	67.5	8.78	190	9.49	7.99	7.35	233.67	0.07	22.22
I19–21/8			19.7	bdl	bdl	23.9	bdl	33.8	65.9	8.55	1500	960	69.3	8.75	160	bdl	10.6	6.74	233.59	0.07	21.65
I19–24/2	Taezhniy	1	20	bdl	bdl	16	bdl	180	85	7.7	2000	860	66	8.9	98	bdl	17	8.2	476.7	0.08	30.3
I19–24/4			11	bdl	bdl	16	bdl	48	85	7.8	2100	1000	70	6.5	120	bdl	14	7.2	559.74	0.07	30
I19–26			7.5	bdl	bdl	15	bdl	37	79	9.2	2500	940	82.8	9.1	130	bdl	11	6.9	480.23	0.09	30.19
I19–26/2			7.4	bdl	bdl	15	bdl	140	75	7.6	2500	910	76.5	11	95	bdl	16	6.9	500.25	0.08	32.68
I19–26/3			20	bdl	bdl	10	2.4	160	120	16	1200	330	223.2	6.2	120	bdl	35	9.1	271.13	0.68	5.38
I19–26/4			bdl	bdl	bdl	30	bdl	92	66	5.8	2000	790	93.6	8.8	120	bdl	12	4.5	509.96	0.12	21.37
I19–26/5			8	bdl	bdl	13	bdl	220	170	18	1900	640	139.5	6.9	150	bdl	34	15	423.69	0.22	13.62
I19–29			5.6	bdl	bdl	19	bdl	220	150	12	1800	670	117	6.3	150	bdl	17	8.4	512.27	0.17	15.38
I19–29/2			17	bdl	bdl	20	bdl	87	110	13	2300	950	82.8	6.7	160	bdl	18	10	538.38	0.09	27.78
I19–29/4			8.1	bdl	bdl	29	bdl	45	71	4.9	2300	720	108	6.1	81	bdl	11	5.2	475.79	0.15	21.3
I19–29/5			6.1	bdl	bdl	38	bdl	190	58	3.3	2700	640	117	11	91	bdl	16	3.7	434.22	0.18	23.08
I19–30/2			16	bdl	bdl	22	bdl	28	76	8.2	2200	910	72	11	130	bdl	12	6.7	529.21	0.08	30.56
I19–30/3			38	bdl	bdl	17	bdl	37	75	8.7	2300	900	94	7.5	120	bdl	12	7	408.88	0.1	24.47
I19–30/4			32	bdl	bdl	21	bdl	230	100	12	2200	980	83.7	6.4	130	bdl	19	8.7	499.86	0.09	26.28
I19–30/5			28	bdl	bdl	19	bdl	140	90	12	2200	1100	73.8	10	160	bdl	32	9	498.3	0.07	29.81
I19–27/2		2	5.1	bdl	bdl	31	bdl	190	42	4.6	1600	770	108	8.7	88	bdl	9.4	3.4	377.4	0.14	14.81
I19–27/7			10	bdl	bdl	17	bdl	48	65	4.4	1900	710	107	8.4	110	bdl	10	4.4	488.85	0.15	17.68
I19–27/3			5.5	bdl	bdl	18	bdl	27	37	2.6	450	230	90	11	190	bdl	7	bdl	473.17	0.39	5
I19–27/4			bdl	bdl	bdl	25	bdl	130	47	4.9	1800	790	117	7.4	110	bdl	7.6	bdl	359.01	0.15	15.38
I19–27/5			5	bdl	bdl	30	bdl	230	45	4.4	1800	730	123	7.1	110	bdl	11	3.2	399.73	0.17	14.69
I19–27/6			5.8	bdl	bdl	31	bdl	280	44	−3.3	1700	610	125	9	100	bdl	11	bdl	407.24	0.2	13.63
I19–28			7.7	bdl	bdl	28	bdl	48	66	4.4	3000	1000	126	12	81	bdl	13	4.7	434.17	0.13	23.81
I19–28/2			bdl	bdl	bdl	30	bdl	47	68	4.1	2200	770	117	7	80	bdl	8.5	bdl	557.68	0.15	18.8
I19–28/3			7.9	bdl	bdl	24	bdl	44	130	9	2300	780	117	5.9	120	bdl	14	7.8	510.85	0.15	19.66
I19–28/4			14	bdl	bdl	19	bdl	67	73	3.6	1700	570	91.8	8	100	bdl	13	3.7	734.28	0.16	18.52

Table A3. Geochemical composition of the igneous rocks of Medvedev and Taezhniy massifs according to ICP-MS data (all values in ppm).

Sample	**I19–22/3**	**I19–22/5**	**M18–9**	**M18–6**	**I19–21/5**	**I-19–7**	**I19–20/2**	**M18–7**	**I19–15**	**I19–24/2**	**I19–24/4**	**I19–30/3**	**I19–27/5**	**I19–27/6**	**I19–27/7**
Massif	Medvedev									Taezhniy					
Phase	1			2		3				1			2		
Rb	103	103	100	71	113	79	80	106	82	66	70	94	123	125	107
Sr	1010	1000	841	1100	917	1030	060	1100	1030	1110	1150	1080	894	759	828
Y	22	23	24	18.7	22	17.2	18.7	22	18.5	16.2	17	22	9.3	8.3	10.5
Zr	157	171	175	138	169	157	130	166	155	130	142	164	119	125	124
Nb	9	9.9	10.1	7.3	8.1	7.4	7.1	7.8	7.3	7	7	8.9	6.5	6.3	6.2
Cs	2.7	4	1.99	4	3.3	3.8	2.7	6.8	5.3	0.85	0.4	0.88	1.25	0.96	0.89
Ba	3130	1970	2150	1880	2050	1860	1810	2060	1980	1910	2060	2220	1830	1660	1590
La	33	40	39	24	35	22	24	32	25	22	23	33	12.7	13.4	14.6
Ce	64	74	71	49	68	46	47	65	52	43	45	64	24	23	28
Pr	7.5	8.7	8.9	6.1	8.4	5.7	6.1	8	6.2	5.3	5.7	7.9	2.9	2.9	3.3
Nd	28	34	33	26	33	23	25	32	25	21	22	30	11.5	10.8	12.9
Sm	5.6	6.3	6.4	5.3	6.8	4.4	5.1	6.3	4.8	4.3	4.5	5.6	2.4	2.3	2.5
Eu	1.52	1.73	1.78	1.43	1.9	1.29	1.37	1.68	1.32	1.11	1.19	1.61	0.66	0.57	0.73
Gd	4.8	5.4	5.7	4.3	5.5	3.9	4.2	5.3	4.3	3.3	3.7	5.2	2.1	1.79	2.2
Tb	0.68	0.71	0.75	0.59	0.76	0.53	0.57	0.7	0.6	0.45	0.52	0.65	0.27	0.24	0.3
Dy	3.7	4.1	4.2	3.3	3.9	2.9	3.3	3.7	3.2	2.7	2.7	3.7	1.44	1.23	1.68
Ho	0.74	0.78	0.84	0.68	0.81	0.6	0.65	0.77	0.65	0.52	0.58	0.7	0.29	0.26	0.33
Er	2	2.2	2.4	1.9	2.2	1.64	1.84	2.1	1.85	1.53	1.61	2.1	0.89	0.78	0.98
Tm	0.33	0.33	0.34	0.27	0.33	0.24	0.27	0.3	0.27	0.23	0.24	0.3	0.14	0.12	0.15
Yb	2	2.2	2.2	1.74	2	1.57	1.74	1.88	1.7	1.5	1.58	1.92	0.94	0.78	1
Lu	0.32	0.32	0.32	0.26	0.31	0.24	0.26	0.28	0.26	0.23	0.23	0.28	0.14	0.12	0.15
Hf	4	4.1	4.3	3.6	4.2	3.9	3.3	4.1	3.8	3.3	3.4	4	3.3	3.3	3.5
Ta	0.4	0.43	0.46	0.34	0.43	0.37	0.34	0.39	0.37	0.34	0.34	0.4	0.28	0.27	0.28
Th	10.3	12.4	12	7.1	9.7	7.4	6.8	8.7	7.7	5.5	6.2	8.9	7.1	5.5	8.6
U	3.2	3.2	3.1	1.65	1.64	1.67	1.84	2.3	1.78	2.2	2.8	3.3	1.65	1.5	1.84
La/Yb	16.01	18	17.84	13.86	17.08	14.17	13.97	17.1	14.98	14.42	14.84	16.93	13.5	17.14	14.58
Ce/Yb	31.57	33.44	32.07	28.39	33.74	28.97	27.16	34.61	30.32	28.9	28.71	33.21	25.83	29.67	28.48
Rb/Sr	0.10	0.10	0.12	0.06	0.12	0.08	0.08	0.10	0.08	0.06	0.06	0.09	0.14	0.16	0.13
Nb/La	0.27	0.25	0.26	0.3	0.23	0.33	0.29	0.24	0.29	0.32	0.3	0.27	0.51	0.47	0.42
Th/U	3.2	3.83	3.93	4.31	5.89	4.43	3.69	3.73	4.34	2.46	2.19	2.66	4.29	3.66	4.69
Y/Nb	2.41	2.33	2.43	2.54	2.77	2.32	2.64	2.78	2.52	2.31	2.43	2.43	1.43	1.33	1.7
Eu/Eu*	0.9	0.91	0.9	0.92	0.95	0.95	0.9	0.88	0.89	0.9	0.88	0.91	0.89	0.85	0.95
∑REE	154.19	180.77	176.83	124.87	168.91	114.01	121.4	160.01	127.15	123.65	130.25	177.95	69.97	66.89	79.69

Table A4. Results of the U-Th-Pb isotopic studies of zircons (SIMS SHRIMP-II) from the igneous rocks of Medvedev and Taezhniy massifs (nd—not detected).

Spot Name	Massif	% comm 206	ppm U	Ppm Th	^{232}Th/^{238}U	ppm Rad ^{206}Pb	^{204}corr ^{206}Pb/^{238}U Age	1s err	% Discordant	Total$^{238/206}$	% err	Total$^{207/206}$	% err	238/206r	% err	207r/206r	% err	207r/235	% err	206r/238	% err	err corr
I19–22 2.1	Medv.	0.06	919	147	0.17	14.3	115.6	1.8	62	55.25	1.6	0.0503	1.4	55.29	1.6	0.050	1.6	0.12	2.2	0.018	1.6	0.704
I19–22 2.2		0.00	1052	148	0.15	17.2	121.2	1.9	−22	52.68	1.6	0.0479	1.3	52.68	1.6	0.048	1.3	0.13	2.1	0.019	1.6	0.765
I19–22 8.1		0.13	665	114	0.18	11.0	123.1	2.0	−39	51.80	1.6	0.0486	1.7	51.87	1.6	0.048	2.1	0.13	2.6	0.019	1.6	0.614
I19–22 9.2		0.21	437	175	0.41	7.1	120.3	2.0	−32	53.00	1.7	0.0493	2.1	53.11	1.7	0.048	2.8	0.12	3.2	0.019	1.7	0.519
I19–22 10.1		7.71	298	96	0.33	5.6	129.9	2.5	310	45.34	1.7	0.1181	1.8	49.13	1.9	0.058	13.6	0.16	13.8	0.020	1.9	0.142
I19–22 11.1		nd	170	65	0.40	2.9	127.2	2.2	38	50.16	1.8	0.0496	3.3	50.16	1.8	0.050	3.3	0.14	3.7	0.020	1.8	0.476
I19–15 2.1	Medv.	0.06	698	7	0.01	11.3	120.2	1.9	−1	53.10	1.6	0.0489	1.7	53.14	1.6	0.048	1.8	1.13	2.4	0.019	1.6	0.672
I19–15 3.1		0.16	447	4	0.01	6.9	114.2	1.9	nd	55.87	1.6	0.0495	2.1	55.96	1.6	0.048	2.6	0.12	3.1	0.018	1.6	0.527
I19–15 4.1		0.08	542	6	0.01	8.9	121.3	2.1	26	52.60	1.7	0.0498	1.9	52.64	1.7	0.049	2.1	0.13	2.7	0.019	1.7	0.640
I19–15 5.1		nd	1020	20	0.02	16.5	120.3	1.9	−31	53.07	1.6	0.0477	1.4	53.07	1.6	0.048	1.4	0.12	2.1	0.019	1.6	0.750
I19–15 6.1		0.13	1237	20	0.02	20.0	119.8	1.9	28	53.22	1.6	0.0501	1.2	53.29	1.6	0.049	1.5	0.13	2.2	0.019	1.6	0.723
I19–15 8.1		0.07	478	4	0.01	7.3	113.5	1.9	3	56.25	1.7	0.0489	2.1	56.29	1.7	0.048	2.2	0.12	2.8	0.018	1.7	0.599
I19–24 3.1	Taezh.	nd	647	38	0.06	10.3	118.4	1.9	38	53.95	1.6	0.0493	1.8	53.95	1.6	0.049	1.8	0.13	2.4	0.019	1.6	0.667
I19–24 4.1		0.05	948	345	0.38	15.0	117.7	1.9	−27	54.23	1.6	0.0481	1.5	54.26	1.6	0.048	1.6	0.12	2.3	0.018	1.6	0.703
I19–24 5.1		0.16	304	122	0.41	4.8	118.2	2.0	−22	53.96	1.7	0.0491	2.6	54.05	1.7	0.048	3.2	0.12	3.6	0.019	1.7	0.471
I19–24 6.1		nd	898	344	0.40	14.3	118.5	1.9	36	53.91	1.6	0.0493	1.5	53.91	1.6	0.049	1.5	0.13	2.2	0.019	1.6	0.726
I19–24 8.1		0.08	1481	101	0.07	23.0	115.6	1.8	−11	55.22	1.6	0.0487	1.2	55.26	.16	0.048	1.4	0.12	2.1	0.018	1.6	0.740
I19–24 9.1		0.06	674	117	0.18	10.6	116.8	1.9	50	54.67	1.6	0.0500	1.8	54.71	1.6	0.050	1.9	0.12	2.5	0.018	1.6	0.652
I19–27–7 3.2	Taezh.	1.85	1678	547	0.34	25.7	114.2	2.0	−9	55.97	1.7	0.0481	1.5	55.97	1.7	0.048	1.5	0.12	2.3	0.018	1.7	0.750
I19–27–7 4.1		0.04	1289	226	0.18	20.4	117.9	2.1	24	54.17	1.8	0.0493	1.7	54.19	1.8	0.049	1.7	0.12	2.5	0.018	1.8	0.716
I19–27–7 7.1		0.13	1926	563	0.30	30.9	119.0	2.1	−6	53.61	1.7	0.0493	1.3	53.68	1.8	0.048	1.6	0.12	2.4	0.019	1.8	0.729
I19–27–7 1.1		0.08	486	2	0.01	7.9	121.0	2.2	20	52.72	1.8	0.0496	2.2	52.76	1.8	0.049	2.4	0.13	3.0	0.019	1.8	0.609
I19–27–7 1.2		1.85	533	14	0.03	8.8	122.9	2.2	5	51.95	1.8	0.0486	2.2	51.95	1.8	0.049	2.2	0.13	2.8	0.019	1.8	0.633
I19–27–7 6.1		0.10	491	27	0.06	8.3	126.1	2.3	8	50.56	1.8	0.0496	2.4	50.61	1.8	0.049	2.6	0.13	3.2	0.020	1.8	0.570
I19–27–7 2.1		0.49	1462	406	0.29	25.1	127.2	2.2	8	49.93	1.8	0.0527	1.4	50.18	1.8	0.049	2.4	0.13	3.0	0.020	1.8	0.590

Table A5. Rb-Sr isotope analyzes the data of rocks of the Medvedev and Taezhniy massifs.

Sample	Massif	Rock	m, gr	Rb, ppm	Sr, ppm	87Rb/86Sr	2σ, %	87Sr/86Sr	2σ, %	2σ, abs.
I19–22/5	Medvedev	Syenite-porphyry	0.10023	100	974	0.29718	0.2	0.708031	0.002	0.000011
I19–21/5		Pyroxene-amphibole syenite	0.10384	113	933	0.34970	0.2	0.707812	0.001	0.000007
I19–15		Quartz monzonite	0.10113	79.4	1338	0.17170	0.2	0.706221	0.001	0.000006
I19–24/2	Taezhniy	Quartz monzonite	0.10628	65.2	1129	0.16710	0.2	0.706457	0.001	0.000008
I19–27/7		Syenite	0.10624	103	851	0.34893	0.2	0.707184	0.001	0.000005

References

1. Bilibin, U.A. Post-Jurassic Intrusions of the Aldan Region. In *Petrography of USSR*; AN USSR: Moscow, Russia, 1941; p. 119. (In Russian)
2. Bilibin, U.A. Mesozoic Igneous Rocks. In *Geology of USSR*; Nedra: Moscow, Russia, 1972; pp. 330–391. (In Russian)
3. Müller, D.; Groves, D.I. Direct and Indirect Associations between Potassic Igneous Rocks, Shoshonites and Gold-Copper Deposits. *Ore Geol. Rev.* **1993**, *8*, 383–406. [CrossRef]
4. Sillitoe, R.H. Characteristics and Controls of the Largest Porphyry Copper-gold and Epithermal Gold Deposits in the Circum—Pacific Region. *Aust. J. Earth Sci.* **1997**, *44*, 373–388. [CrossRef]
5. Müller, D. Gold-Copper Mineralization in Alkaline Rocks. *Miner. Depos.* **2002**, *37*, 1–3. [CrossRef]
6. Sillitoe, R. Some Metallogenic Features of Gold and Copper Deposits Related to Alkaline Rocks and Consequences for Exploration. *Miner. Depos.* **2002**, *37*, 4–13. [CrossRef]
7. Bissig, T.; Cooke, D.R. Introduction to the Special Issue Devoted to Alkalic Porphyry Cu-Au and Epithermal Au Deposits. *Econ. Geol.* **2014**, *109*, 819–825. [CrossRef]
8. Soloviev, S.G. *Metallogeny of Shoshonite Magmatism. v.1,2.*; Science World: Moscow, Russia, 2014.
9. Müller, D.; Groves, D.I. Mineral Resource Reviews. In *Potassic Igneous Rocks and Associated Gold-Copper Mineralization*; Springer International Publishing: Cham, Switzerland, 2019; ISBN 978-3-319-92978-1.
10. Wolfe, R.C.; Cooke, D.R. Geology of the Didipio Region and Genesis of the Dinkidi Alkalic Porphyry Cu-Au Deposit and Related Pegmatites, Northern Luzon, Philippines. *Econ. Geol.* **2011**, *106*, 1279–1315. [CrossRef]
11. Zhang, Y.; Qiu, E.; Dong, S.; Li, J.; Shi, W. Late Mesozoic Intracontinental Deformation and Magmatism in North and NE China in Response to Multi-Plate Convergence in NE Asia: An Overview and New View. *Tectonophysics* **2022**, *835*, 229377. [CrossRef]
12. Belyaev, G.M.; Rudnick, V.A. *Formation-Genetic Types of Granitoids*; Nedra: St. Petersburg, Russia, 1978. (In Russian)
13. Kuznetcov, V.A. *Ore-Formation Analysis and Metallogeny Problems*; Nauka: Novosibirsk, Russia, 1988. (In Russian)
14. Ponomarchuk, A.V.; Prokopyev, I.R.; Doroshkevich, A.G.; Semenova, D.V.; Kravchenko, A.A.; Ivanov, A.I. Geochronology of the Mesozoic Alkaline Magmatism of Tyrkanda and Amga Tectonic Zones (Aldan Shield): New U-Pb and Ar-Ar Data. *Geosfernye Issled* **2020**, *4*, 6–24. (In Russian) [CrossRef]
15. Maksimov, E.P.; Uytov, V.I.; Nikitin, V.M. Central-Aldan Gold-Uranium Ore Magmatogenic System (Aldano-Stanovoy Shield, Russia). *Pac. Geol.* **2010**, *29*, 3–26. (In Russian)
16. Trunilina, V.A.; Roev, S.P.; Et, A. *Magmatism of Various Geodynamic Settings (the Joint Zone of the Verkhoyansk Margin of the Siberian Continent and the Kolyma-Omolon Microcontinent)*; YSC SB RAS: Yakutsk, Russia, 1999. (In Russian)
17. Parfenov, L.M.; Kuzmin, M.I. (Eds.) *Tectonics, Geodynamics, and Metallogeny of the Territory of the Sakha Republic (Yakutia) (in Russian)*; Nauka/Inte.; MAIK "Nauka"/ Interperiodika: Moscow, Russia, 2001. (In Russian)
18. Ivanov, A.; Ivanov, M.; Zhuravlev, A. Petrography of the Mesozoic Alkaline Rocks of the Medvedev Massif (South Yakutia, Aldan-Stanovoy Shield, Leglier Ore Cluster). *IOP Conf. Ser. Earth Environ. Sci.* **2020**, *609*, 012003. [CrossRef]
19. Bilibin, U.A. *Favorite Publications*; AN USSR: Moscow, Russia, 1958; Volume 1. (In Russian)
20. Vetluzhskikh, V.G.; Kazanskii, V.I.; Kochetkov, A.Y.; Yanovskii, V.M. Gold-ore deposits of the Central Aldan. *Geol. ore Depos.* **2002**, *44*, 467–499. (In Russian)
21. Kochetkov, A.Y. Mesozoic Gold-Bearing Ore-Magmatic Systems of Central Aldan. *Russ. Geol. Geofiz.* **2006**, *47*, 850–864. (In Russian)
22. Dvornick, G.P. Gold-Ore Metasomatic Formations of the Central-Aldan Region. *Lithosphere* **2012**, *2*, 90–105. (In Russian)
23. Terekhov, A.V. *Ore Potential of Hydrothermal-Metasomatic Formations of the E'kon Gold-and-Uranium Ore Cluster (South Yakutia)*; VSEGEI: St. Petersburg, Russia, 27 September 2012. (In Russian)
24. Shatova, N.V. *Ore Potential of Hydrothermal-Metasomatic Formations of the Ryabinovoe Ore Field (South Yakutia)*; VSEGEI: St. Petersburg, Russia, 2018. (In Russian)
25. Molchanov, A.V.; Terekhov, A.V.; Shatov, V.V.; Petrov, O.V.; Kukushkin, K.A.; Kozlov, D.S.; Shatova, N.V. Gold Ore Districts and Ore Clusters of the Aldanian Metallogenic Province. *Reg. Geol. Metallog.* **2017**, *71*, 93–111. (In Russian)
26. Ivanov, M.; Ivanov, A.; Zhuravlev, A. Petrography of the Mesozoic Alkaline Rocks of the Taezhniy Massif (South Yakutia, Aldan-Stanovoy Shield, Leglier Ore Cluster). *IOP Conf. Ser. Earth Environ. Sci.* **2021**, *906*, 012115. [CrossRef]
27. Rad'kov, A.V.; Molchanov, A.V.; Artemiev, D.S.; Belenko, E.V. *State Geological Map of the Russian Federation*; Cartographic factory of VSEGEI: St. Petersburg, Russia, 2015. (In Russian)

28. Schuth, S.; Gornyy, V.I.; Berndt, J.; Shevchenko, S.S.; Karpuzov, A.F.; Mansfeldt, T. Early Proterozoic U-Pb Zircon Ages from Basement Gneiss at the Solovetsky Archipelago, White Sea, Russia. *Int. J. Geosci.* **2012**, *03*, 289–296. [CrossRef]
29. Williams, I.S. U-Th-Pb Geochronology by Ion Microprobe ABOUT TIME. *Rev. Econ. Geol.* **1998**, *7*, 1–35.
30. Ludwig, K.R. *SQUID 1.02, a User Manual, a Geochronological Toolkit for Microsoft Excel*; Berkeley Geochronology Center Special Publication: Berkeley, CA, USA, 2001.
31. Black, L.P.; Kamo, S.L.; Allen, C.M.; Aleinikoff, J.N.; Davis, D.W.; Korsch, R.J.; Foudoulis, C. TEMORA 1: A New Zircon Standard for Phanerozoic U-Pb Geochronology. *Chem. Geol.* **2003**, *200*, 155–170. [CrossRef]
32. Wiedenbeck, M.; Alle, P.; Corfu, F.; Griffin, W.L.; Meier, M.; Oberli, F.; Von Quadt, A.; Roddick, J.C.; Spiegel, W. Three natural zircon standards for U-Th-Pb, Lu-Hf, trace element and REE analyses. *Geostand. Newsl.* **1995**, *19*, 1–23. [CrossRef]
33. Wetherill, G.W. Discordant Uranium—Lead Ages, I. *Eos Trans. Am. Geophys. Union* **1956**, *37*, 320–326. [CrossRef]
34. Ludwig, K.R. Berkeley Geochronology Center Special Publication No.4. Components. In *User's Manual for Isoplot 3.00, a Geochronological Toolkit for Microsoft Excel*; Berkeley Geochronology Center Special Publication: Berkeley, CA, USA, 2003.
35. Stacey, J.S.; Kramers, J.D. Approximation of Terrestrial Lead Isotope Evolution by a Two-Stage Model. *Earth Planet. Sci. Lett.* **1975**, *26*, 207–221. [CrossRef]
36. Le Maitre, R.W.; Streckeisen, A.; Zanettin, B.; Le Bas, M.J.; Bonin, B.; Bateman, P. (Eds.) *Igneous Rocks: A Classification and Glossary of Terms*, 2nd ed.; Cambridge University Press: Cambridge, UK, 2002; ISBN 9780511535581.
37. Wilson, M. Review of igneous petrogenesis: Aglobal tectonic approach. *Terra Nov.* **1989**, *1*, 218–222. [CrossRef]
38. De la Roche, H.; Leterrier, J.; Grandclaude, P.; Marchal, M. A Classification of Volcanic and Plutonic Rocks Using R1R2-Diagram and Major-Element Analyses—Its Relationships with Current Nomenclature. *Chem. Geol.* **1980**, *29*, 183–210. [CrossRef]
39. Whitford, D.J.; Nicholls, I.A.; Taylor, S.R. Spatial Variations in the Geochemistry of Quaternary Lavas across the Sunda Arc in Java and Bali. Contrib. *Mineral. Petrol.* **1979**, *70*, 341–356. [CrossRef]
40. Tauson, L.V.; Gundobin, G.M.; Zorina, L.D. *Geochemical Fields of Ore-Magmatic Systems*; Nauka: Novosibirsk, Russia, 1987. (In Russian)
41. Sun, S.S.; McDonough, W.F. Chemical and Isotopic Systematics of Oceanic Basalts: Implications for Mantle Composition and Processes. *Geol. Soc. Spec. Publ.* **1989**, *42*, 313–345. [CrossRef]
42. Cox, K.G.; Bell, J.D.; Pankhurst, R.J. *The Interpretation of Igneous Rocks*; Springer: Dordrecht, The Netherlands, 1979; ISBN 978-0-412-53410-2.
43. Tischendorf, G.; Palchen, W. Zur Klassification von Granitoiden. *Z. Fuer Geol. Wiss.* **1985**, *13*, 615–627.
44. Frost, B.R.; Barnes, C.G.; Collins, W.J.; Arculus, R.J.; Ellis, D.J.; Frost, C.D. A Geochemical Classification for Granitic Rocks. *J. Petrol.* **2001**, *42*, 2033–2048. [CrossRef]
45. Pearce, J.A.; Harris, N.B.W.; Tindle, A.G. Trace Element Discrimination Diagrams for the Tectonic Interpretation of Granitic Rocks. *J. Petrol.* **1984**, *25*, 956–983. [CrossRef]
46. Maniar, P.D.; Piccoli, P.M. Tectonic Discrimination of Granitoids. *Geol. Soc. Am. Bull.* **1989**, *101*, 635–643. [CrossRef]
47. Müller, D.; Rock, N.M.S.; Groves, D.I. Geochemical Discrimination between Shoshonitic and Potassic Volcanic Rocks in Different Tectonic Settings: A Pilot Study. *Mineral. Petrol.* **1992**, *46*, 259–289. [CrossRef]
48. Datsenko, V.M. Petrogeochemical Typification of Granitoids of the Southwestern Framing of the Siberian Platform. In Proceedings of the II Whole-Russia Petrographic Symposium, 2000, Syktyvkar, Russia, 27–30 June 2000; pp. 270–274. (In Russian).
49. Sergeev, S.A.; Pushkarev, Y.D.; Lohov, K.I.; Sergeev, D.S. *Obzor Sovremennykh Metodov Izotopnoy Geokhronologii (Sostavnaya Chast' Geokhronologicheskogo Atlasa) 95/5 000* Результаты Перевода *Review of Modern Methods of Isotope Geochronology (Part of the Geochronological Atlas)*; VSEGEI: St. Petersburg, Russia, 2015. (In Russian)
50. Rub, M.G.; Gladkov, N.G.; Pavlov, V.A.; Rub, A.K.; Troneva, N.V. Alkaline Elements and Strontium in Ore-Bearing (Sn, W, Ta) Differentiated Igneous Associations. *Dokl. Earth Sci.* **1984**, *268*, 1463–1466. (In Russian)
51. Lightfoot, P.C.; Howkesworth, C.J.; Hergt, J.; Et, A. Remobilisation of the Continental Lithosphere by a Mantle Plume: Major Trace-Element, and Sr-, Nd-, and Pb-Isotopic Evidence from Picritic and Tholeiitic Lavas of the Noril'sk District, Siberian Trap, Russia. *Contrib. Mineral. Petrol.* **1993**, *114*, 171–188.
52. Taylor, S.R.; McLennan, S.M. *The Continental Crust: Its Composition and Evolution*; Blackwell Scientific Publications: Oxford, MS, USA, 1985.
53. Balashov, Y.A. *Geochemistry of Rare-Earth Elements*; Nauka: Moscow, Russia, 1976. (In Russian)
54. Rudnick, R.L.; Gao, S. Composition of the Continental Crust. In *Treatise on Geochemistry*; Elsevier Inc.: Amsterdam, The Netherlands, 2003; Volume 3–9, pp. 1–64, ISBN 9780080548074. [CrossRef]
55. Sasim, S.A. *Shoshonite-Latite and Trachybasalt Series of Eastern Transbaikalia: Isotope-Geochemical Features and Genesis of Igneous Rocks of the Alexander-Zavodsk Depression*; Institute of Geochemistry: Irkutsk, Russia, 2012.
56. Gusev, A.I. *Petrology of Gold-Forming Magmatism*; Natural Sciences Academy: Moscow, Russia, 2012. (In Russian)
57. Mair, J.L.; Farmer, G.L.; Groves, D.I.; Hart, C.J.R.; Goldfarb, R.J. Petrogenesis of Postcollisional Magmatism at Scheelite Dome, Yukon, Canada: Evidence for a Lithospheric Mantle Source for Magmas Associated with Intrusion-Related Gold Systems. *Econ. Geol.* **2011**, *106*, 451–480. [CrossRef]
58. Stepanov, V.A. Bamskoe Gold-Ore Deposit (Stanovoy Ridge, Russia). *Geol. ore Depos.* **2001**, *43*, 38–51. (In Russian)
59. Djenshuraeva, R. Middle Tien-Shan Backarc Magmatic Belt and Gold Deposits. In *Understanding the Genesis of Ore Deposits to Melt the Demands of the 21-st Quadrennial IAGOD Symposium*; Informpoligraph: Moscow, Russia, 2006; pp. 147–148. (In Russian)

60. Maksimov, E.P. *Mesozoic Ore-Bearing Magmatogenic Systems of Aldan-Stanovoy Shield*; Neryungri Printing House: Neryungri, Russia, 2003. (In Russian)
61. Kochetkov, A.Y.; Lazebnick, K.A. Alkaline Ultrabasic and Basic Rocks of Yakokut Massif (Central Aldan). In *Geochemistry and Mineralogy of Basalts and Ultrabasites of Siberian Platform*; SBASUSSR: Yakutsk, Russia, 1984; pp. 62–82. (In Russian)
62. Kononova, V.A.; Pervov, V.A.; Bogatikov, O.A.; Myus-Shumaher, U.; Keller, I. Mesozoic Potassium Mamatism of Central Aldan: Geodynamics and Genesis. *Geotectonics* **1995**, *3*, 35–45. (In Russian)
63. Rokosova, E.U. *Composition and Characteristics of Melt Crystallization during the Formation of Potassium Mafic Rocks of the Central Aldan (on the Example of the Yllimakh, Ryabinovskii and Inagli Massifs)*; IGM: Novosibirsk, Russia, 2014. (In Russian)
64. Donskaya, T.V.; Gladkochub, D.P.; Mazukabzov, A.M.; Ivanov, A.V. Late Paleozoic—Mesozoic Subduction-Related Magmatism at the Southern Margin of the Siberian Continent and the 150 Million-Year History of the Mongol-Okhotsk Ocean. *J. Asian Earth Sci.* **2013**, *62*, 79–97. (In Russian) [CrossRef]
65. Leeman, W.; Worner, G.; Churikova, T.; Tonarini, S.; Heuser, A. Boron and Fluid-Mobile Element (FME) Fluxes Across Kamchatka. *J. Conf. Abstr. EUG 11* **2001**, *6*, 391.
66. Kudrin, M.V.; Fridovsky, V.Y.; Polufuntikova, L.I.; Kryuchkova, L.Y. Disseminated Gold–Sulfide Mineralization in Metasomatites of the Khangalas Deposit, Yana–Kolyma Metallogenic Belt (Northeast Russia): Analysis of the Texture, Geochemistry, and S Isotopic Composition of Pyrite and Arsenopyrite. *Minerals* **2021**, *11*, 403. [CrossRef]
67. Ivanov, M.S.; Ivanov, A.I.; Loskutov, E.E.; Zhuravlev, A.I. Mafic Minerals of the Medvedev Massif (South Yakutia). In Proceedings of the X international siberian early career geoscientists conference, Novosibirsk, Russia, 13–17 June 2022; pp. 93–94. (In Russian).